CO$_2$ flux characteristics of the grassland ecosystem and its response to environmental factors in the dry-hot valley of Jinsha River, China

Chaolei Yang[a,b,c,d], Yufeng Tian[a,b,c,d,*], Jingqi Cui[e], Guangxiong He[f], Jingyuan Li[e],
Canfeng Li[a,b,c], Haichuang Duan[a], Zong Wei[a,b], Liu Yan[a,b], Xin Xia[a,b], Yong Huang[a,b],
Aihua Jiang[a,b], and Yuwen Feng[g]

[a] Kunming General Survey of Natural Resources Center, China Geological Survey, Kunming, 650111, China

[b] Yunnan Province Field Science Observation and Research Station on the Evolution of Soil and Water Resources and the Carbon Sequestration Enhancement Effects in the Alpine Gorge Area of the Jinsha River, Chuxiong, 651400, China

[c] Technology Innovation Center for Natural Carbon Sink, Kunming, 650111, China

[d] Key Laboratory of Coupling Process and Effect of Natural Resources Elements, Beijing, 100055, China

[e] Institute of Space Weather, School of Atmospheric Physics, Nanjing University of Information Science and Technology, Nanjing, 210044, China

[f] Tropical Eco-Agriculture Research Institute, Yunnan Academy of Agricultural Sciences, Chuxiong, 651300, China

[g] Bazhong Meteorological Office of Sichuan Province, Bazhong, 636000, China

Correspondence to: Yufeng Tian (yufeng_tian818@126.com)

ABSTRACT: The savanna ecosystem in the dry-hot valley of the Jinsha River is a unique non-zonal heat island habitat in the global temperate region. As a key component of this ecosystem, even minor changes in the CO$_2$ flux of grasslands can significantly impact the carbon budget of the area. However, there is currently a lack of field monitoring data and related research reports. To reveal the dynamic characteristics of grassland CO$_2$ flux in the Jinsha River dry-hot valley and to quantitatively assess the annual CO$_2$ flux, this study conducted long-term fixed-point observations of CO$_2$ flux changes in grasslands using the static chamber method. Additionally, the effects of various environmental factors on CO$_2$ flux were examined, and the variations in grassland CO$_2$ flux under future drought and rainless climate scenarios were also analyzed. The results showed that during the dry season, the grassland in the Jinsha River dry-hot valley exhibited a carbon emission state, with an average daily CO$_2$ flux of 0.1632 $\mu mol \cdot m^{-2} \cdot s^{-1}$ and a cumulative CO$_2$ emission of 1.3215 $t \cdot ha^{-1}$. In contrast, during the rainy season, the grassland demonstrated significant carbon absorption characteristics, with an average daily CO$_2$ flux of -0.1062 $\mu mol \cdot m^{-2} \cdot s^{-1}$ and a cumulative CO$_2$ absorption of 0.6137 $t \cdot ha^{-1}$. From a yearly perspective, the grassland ecosystem acted as a weak carbon source, with an annual cumulative CO$_2$ emission of 0.7078 $t \cdot ha^{-1} \cdot a^{-1}$, exhibiting carbon-neutral characteristics. In terms of environmental factors, the influence of temperature factors on the variation of CO$_2$ flux in the grassland was generally weak, which was related to the small temperature differences at different time scales in the study area. Precipitation primarily controlled

the variation of CO_2 flux in the grassland indirectly by affecting soil moisture content and relative humidity. When soil water content was at the dry and intermediate periods, the net ecosystem carbon exchange of the grassland significantly decreased with increasing soil water content. However, when soil water content exceeded a certain threshold, further increases in soil moisture lead to an increase in net ecosystem carbon exchange. Additionally, reductions in relative humidity and increases in vapor pressure deficit also suppressed the carbon absorption capacity of the grassland. Overall, under future scenarios of sustained drought and low precipitation, the CO_2 emissions from the grassland ecosystem in the Jinsha River dry-hot valley may continue to rise.

Key words: dry-hot valley of Jinsha River; savanna; grassland ecosystem; CO_2 flux; environmental factors

1 Introduction

Since the industrial revolution, human economic and social progress heavily relied on fossil energy consumption. The excessive emissions of greenhouse gases such as CO_2 have been considered to be the main cause of increased atmospheric CO_2 concentration and global warming (Sha et al., 2022; Wang et al., 2023).The terrestrial ecosystem can absorb about 15.0%–30.0% of anthropogenic CO_2 emissions per year, and the carbon (C) neutrality capacity index reaches 27.14% (Green et al., 2019; Bai et al., 2023; Liu et al., 2023; Zeng et al., 2023). This makes it a significant C sink (Piao et al., 2018; Yang et al., 2022). Studying the dynamic changes in the C budget of global terrestrial ecosystems, along with their environmental driving factors, has become an important topic in the field of global change (Houghton, 2001; Bai et al., 2023). Grasslands cover about 40.5% of the global land surface and are a crucial component of terrestrial ecosystems (Bai et al., 2022). Their carbon storage (CS) accounts for approximately 1/3 of the total terrestrial CS worldwide, which is equivalent to that of forest ecosystems and significantly influences the global C balance (White et al., 2000; Wang et al., 2021).

The savanna ecosystems cover 1/6 of the Earth's total land area (Grace et al., 2006), which ecosystem structure and vegetation community composition are significantly controlled by hydrological conditions (Yu et al., 2015; Lee et al., 2018; Jin et al., 2019; Zhang et al., 2019; Hoffmann, 2023) and are composed of mixed forest and grassland ecosystems. The vegetation is mainly composed of grass, with sparse distribution of trees and shrubs. Being a significant component of the worldwide grassland ecosystem, its net primary productivity (NPP) accounts for about 30.0% of the total NPP of terrestrial ecosystems, which has significant impacts on global

material cycling, energy flow, and climate change (Grace et al., 2006; Peel et al., 2007; Dobson et al., 2022). Grace et al. (2006) indicated that the herbaceous plants in the savanna ecosystem are mainly C_4 grasses, but only moderate productivity, the average NPP was 7.2 ± 2.0 t C ha^{-1}·a^{-1}, and the CO_2 flux (Fc) of the savanna ecosystem has significantly different characteristics in the dry season and the rainy season. The rainy season is mainly dominated by C absorption, and the maximum net rate of C fixation can reach 2/3 of the maximum value of the tropical rainforest (Grace et al., 2006). The dry season is marked by weak C emission or weak C sinks (Grace et al., 1995; Malhi., 1998; Saleska et al., 2003; Bousquet et al., 2006; Millard et al., 2008; Livesley et al., 2011; Fei et al., 2017a). Furthermore, in the tropical savanna ecosystem, grass-derived C contributes to over half of the total soil organic carbon (SOC) in the soil up to a depth of 1 meter, even in the soil under the tree, that is, the C in the soil mainly comes from herbaceous plants (Zhou et al., 2023). Simultaneously, since the savanna ecosystem mainly stores C in the soil rather than the biomass of trees, some researchers have suggested that it may emerge as a more significant C sink resource than forests in the future (Dobson et al., 2022).

The savanna ecosystem in China is mainly manifested as the ecological landscape of the valley-type sparsely shrub-grass vegetation distributed in the special geographical unit of the dry-hot valley, which is similar to the tropical savannas, it belongs to the open savanna ecosystem. It is also known as valley-type savanna vegetation or semi-savanna vegetation (Jin et al., 1987; Shen et al., 2010). It is mainly distributed in the Yuanjiang (YJ), Nu River, and Jinsha River (JS), and their tributaries in southwest China. The ecosystem is characterized by low annual rainfall, high average annual temperature, and high evaporation. The species richness increases with altitude (He et al., 2024), which belongs to the non-zonal special hot island habitat evolved from the global temperate humid climate zone (Zhang, 1992). It is an ideal location for studying changes in plant carbon budget under sustained drought and high-temperature climate conditions. At present, there are limited studies on the C balance of the valley-type savanna ecosystem in the dry-hot valley of China. The existing studies primarily concentrate on the YJ. In the investigation of soil respiration dynamics in the savanna ecosystem of the YJ, Yang et al. (2020) found that the annual total C emission from soil respiration in this region is relatively low compared to global savanna ecosystems, at 4.20 t·ha^{-1}·a^{-1}. Fei et al. (2017a) revealed that the savanna ecosystem of the YJ was a C sink, and about 84.0% of the C sinks was mainly concentrated in the rainy season (1.08 ± 0.35 t C ha^{-1}), and the dry season was C neutral. With expected increase in temperatures and unpredictable rainfall events driven by climate change, this ecosystem's C sink ability could potentially decrease. The dry-hot valley of JS is the largest dry-hot valley in China, and it is also a typical representative of the valley-type savanna

104 ecosystem in China. However, monitoring and research on the F_c features in this region is still

105 lacking.

106   Similar to the tropical savanna ecosystem, grassland ecosystems play an important role in the

107 dry-hot valley savanna ecosystem in JS and are a key component of the plant community in this

108 region. Even small dynamic changes in grassland F_c will significantly affect the C balance of the

109 entire valley-type savanna ecosystem and the surrounding area. This study focuses on the grassland

110 ecosystem in the dry-hot valley of JS, using the static chamber method to observe the F_c of the

111 grassland. The aim is to clarify the dynamic characteristics of grassland F_c and its correlation with

112 environmental factors, quantitatively assess the annual F_c of the grassland, and attempt to address

113 the trends of F_c changes in the dry-hot valley grasslands under future drought and low precipitation

114 climate scenarios. This is done to offer a scientific reference for in-depth comprehension of the key

115 processes of carbon cycle in the valley-type savanna in China, and to study and predict the

116 ecological function changes of vegetation carbon sequestration under continuous drought and high

117 temperature stress in the future.

2 Data and methods

2.1 Observation sites

120   All observational data were derived from the Jinsha River Field Observation Station

121 (26°4'6.24" N, 101°49'41.68" E), whose test site is situated in the Shikanzi Daqing River Basin on

122 the west bank of JS (Fig. 1), with a representative savanna ecological landscape. The elevation of

123 the basin is 1200–1800 m, falling within the realm of the southern subtropical dry-hot monsoon

124 climate, with the characteristics of drought, high temperature and less rain. The ecosystem is

125 extremely fragile and sensitive. The annual average temperature is 22.93°C, with daily maximum

126 temperatures reaching over 43.00°C. The region has distinct rainy season (June to October) and dry

127 season (November to May of the subsequent year), and the annual precipitation is 428.50 mm, with

128 over 90.0% of the precipitation concentrated in the rainy season. The annual evaporation rate is high,

129 typically 3–6 times the annual precipitation (He et al., 2000). Herbaceous plants are mainly

130 *Heteropogon contortus* (Linn.) Beauv., *Eulaliopsis binate* (Retz.) C. E. Hubb, *Cymbopogon*

131 *goeringii* (Steud.) A. Camus, *Eulalia speciosa* (Debeaux) Kuntze, and so on. The shrubs include

132 *Phyllanthus emblica* L., *Pistacia weinmannifolia* J. Poisson ex Franch, *Quercus franchetii* Skan,

133 *Quercus cocciferoides* Hand. –Mazzz, *Dodonaea viscosa* (L.) Jacq., *Albizia kalkora* (Roxb.) Prain,

134 *Osteomeles schwerinae* Schneid., *Osyris wightiana*, and *Terminalia franchetii* Gagnep. , etc.

2.2 Data source

2.2.1 Micrometeorological Factor Observation

The micro-meteorological factors were continuously monitored in real-time by the DL3000 small automatic meteorological observation system deployed in the test site of the observation station. The observation time began on January 12, 2023, and the observation indexes included air temperature (Ta), relative humidity (RH), soil temperature (Ts), soil water content (SWC), soil conductivity (SC), precipitation (P), wind speed (Ws), wind direction (WD), and photosynthetically active radiation (PAR). The average value of the environmental factors observation data for 5 minutes, 30 minutes, and 24 hours are automatically recorded through the CR1000X data logger. The specific meteorological observation system sensor equipment information is listed in Table 1.
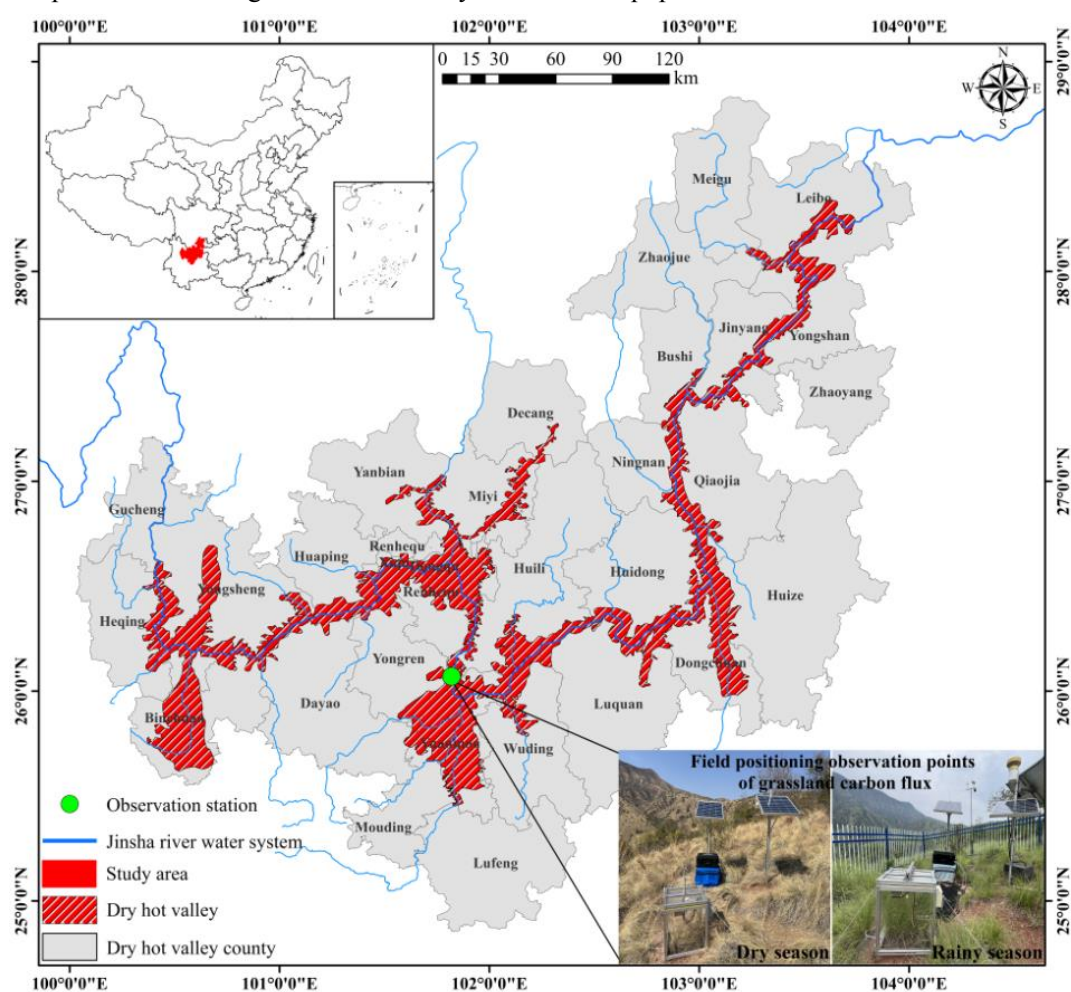

Figure 1 Range of dry-hot valley in JS and location of the Jinsha River Field Observation Station.

2.2.2 CO_2 flux observation

In order to ensure the representativeness of the observation plots and the spatial integration of the observation data, the typical grassland plots with small micro-habitat differences were selected in the test site of the observation station to lay out and install static assimilative boxes for positioning observation. The observation point is about 10 meter away from the automatic meteorological

observation system. The observation time began at 3:05 PM on March 3, 2023, and ended at 10:50 AM on November 1, 2023. The bottom area of the assimilative box is 0.25 m², and the volume in the box is 125 L. The whole box is composed of transparent organic glass. There are two sets of fans in the box, which can fully mix the gas evenly. The height of the base is 8cm, embedded in the underground soil is 5 cm, and the aboveground part is 3 cm. The net ecosystem carbon exchange (NEE) was mainly measured by the CARBOCAP ® C dioxide sensor GMP343 of Vaisala Company. The diffusion probe of the sensor can effectively reduce the measurement error caused by the pressure difference of the pumping system. It has the characteristics of flexibility and high precision and is widely used in ecosystem CO_2 monitoring (Harmon et al., 2015). The top cover of the assimilative box can be automatically opened and closed, and the time of a single complete measurement cycle is 15 minutes. Before the measurement, the top cover of the assimilative box will be automatically opened, so that the gas in the box and the surrounding air are mixed evenly, and the time is 5 minutes. Then the top cover of the box is automatically closed to a closed and stable state, the fan starts, and the gas change in the box is measured. The measurement and recording time is 10 minutes, so repeated.

Table 1 Information of micrometeorological observation system.

Name of instrument	Manufacturer	Observation parameter	Height (depth) of installation (m)
Temperature and humidity sensor	Campbell	Ta (°C) and RH (%)	1.5
Photosynthetic effective radiometer	Campbell	PAR (μmol·m^{-2}·s^{-1})	1.5
Wind speed and direction sensor	Campbell	Ws (m/s) and WD (°)	1.5
Rainfall sensor	Campbell	P (mm)	1.5
Soil multi-parameter sensor	Campbell	Ts (°C), SWC (m³ · m^{-3}), and SC (dS/m)	Soil horizon 0.1

2.2.3 Other data

The boundary data of the dry-hot valley was sourced from Deng (2022). The administrative boundary data (Xu, 2023a; Xu, 2023b) and river data (Xu, 2018) were sourced from the Resources and Environment Science Data Center (RESDC) from the Chinese Academy of Sciences.

2.2.4 Data processing

When the Fc is measured, the whole monitoring system will collect the original data of GMP343 at a speed of 2 Hz through the CR1000X data logger, and average the data collected within 5 seconds for statistical analysis (main scan interval). If the difference between the newly acquired data and the average value exceeds 8 times the standard deviation, it is classified as an outlier, and

177 such data points are eliminated. The system performs linear regression fitting on the removed data

178 and calculates the ecosystem CO_2 exchange capacity, goodness of fit, etc.

179   The ecosystem CO_2 exchange capacity is calculated by the formula (1):

180
$$F_c = \frac{V \times P_{av} \times (1000 - W_{av})}{R \times S \times (T_{av} + 273)} \times \frac{\partial_c}{\partial_t} (1)$$

181 where F_c represents CO_2 flux ($\mu mol \cdot m^{-2} \cdot s^{-1}$); V represents the volume of assimilative chamber (m^3);

182 P_{av} represents the mean atmospheric pressure (kPa) inside the chamber during the observation

183 period; W_{av} represents the partial pressure of water vapor inside the chamber during the observation

184 period ($mmol \cdot mol^{-1}$); R represents the atmospheric constant ($8.314 \ J \cdot mol^{-1} \cdot K^{-1}$); S represents the

185 area of assimilative chamber (m^2); ∂_c / ∂_t represents the diffusion rate of CO_2 in the chamber; T_{av}

186 represents the mean temperature (°C) inside the chamber during the observation period.

187   The linear regression method was employed to fit the CO_2 diffusion rate (∂_c / ∂) (formula 2).

188 This method is the basic method for measuring the CO_2 diffusion rate of most soil respiration and

189 is widely used (Wen et al., 2007):

190
$$c(t) = c + \frac{\partial_c}{\partial_t} t \ (2)$$

191 where $c(t)$ represents the CO_2 concentration within the assimilative chamber; t represents the

192 determination time; c represents the CO_2 concentration in the assimilative chamber when it is closed.

193   Taking into account the specific conditions of the study area, the recorded Fc data was

194 categorized into dry season (March 3rd–May 31st) and rainy season (June 1st–November 1st). Due

195 to the damage of the assimilative box from June 1st to August 6th and the lack of observation data,

196 considering the continuity of the data time series and the precision of the data, the dry season Fc

197 data is mainly based on the observation data from March 4th to May 31st, and the rainy season Fc

198 data is mainly based on the observation data from August 7th to October 31st. Quality control was

199 conducted on the raw data to remove invalid NAN values and abnormal data (the abnormal data

200 mainly consisted of negative values during the dry season and negative values at night during the

201 rainy season). Utilizing the research results from Zhao et al. (2020), missing data points with a time

202 difference of under 3 hours are filled in using linear interpolation. For data with a missing duration

203 of more than 3 hours, interpolation is mainly performed by distinguishing between daytime and

204 nighttime periods. Among them, the data of daytime in the rainy season were interpolated by

205 formula (3) rectangular hyperbolic model (Ruimy et al., 1995) to simulate the relationship between

206 NEE and PAR. The missing data of the rainy season at nighttime and the dry season were

207 interpolated by the multiplicative model (4) of the response of ecosystem respiration to Ts and SWC:

208
$$NEE_{daytime} = R_{daytime} - \frac{A_{max} \times \alpha \times PAR_{daytime}}{A_{max} + \alpha \times PAR_{daytime}} (3)$$

209   where $NEE_{daytime}$ represents the NEE during the daytime ($\mu mol \cdot m^{-2} \cdot s^{-1}$); A_{max} represents the

210   maximum photosynthetic rate ($\mu mol \cdot m^{-2} \cdot s^{-1}$); α represents the apparent quantum efficiency

211   ($\mu mol \cdot mol^{-1}$); $R_{daytime}$ represents the daytime ecosystem respiration rate ($\mu mol \cdot m^{-2} \cdot s^{-1}$); $PAR_{daytime}$

212   represents the PAR during the daytime ($\mu mol \cdot m^{-2} \cdot s^{-1}$).

213
$$ER = a \times e^{\beta T_s} \times SWC^C \quad (4)$$

214   where ER represents the ecosystem respiration rate ($\mu mol \cdot m^{-2} \cdot s^{-1}$); α, β and c represents the fitting

215   parameters; Ts and SWC are shown in Table 1.

216   The vapor pressure deficit (VPD) is calculated by formula (5) (Campbell et al., 2012):

217
$$VPD = 0.61078 e^{\frac{17.27 Ta}{Ta+237.3}} (1 - RH) \quad (5)$$

218   where RH and Ta are shown in Table 1.

219 3 Analysis of the effect

220 3.1 Dynamic changes in environmental factors

221   Utilizing the observational data of micrometeorological factors, the dynamic attributes of

222   environmental factors such as Ta, VPD, RH, P, Ws, PAR, Ts and SWC. It can be seen that these

223   environmental factors showed a high degree of seasonal characteristics, especially the P and SWC

224   were the most obvious. Among them, the P in the rainy season was 400.80 mm, mainly concentrated

225   in August (142 mm). The precipitation frequency was 17 times, and the SWC changed between 0–

226   0.19 $m^3 \cdot m^{-3}$, also showing a strong response relationship with P (Fig. 2a and 2b). The minimum RH

227   was 20.65% and the maximum was 94.10%, showing a strong response relationship with P. The

228   VPD fluctuated between 0.11–4.13 kPa, and its value decreased significantly after May, which was

229   related to the increase of P and RH in the rainy season (Fig. 2a and 2c). During the observation

230   period, the PAR varied from 52.28–860.59 $\mu mol \cdot m^{-2} \cdot s^{-1}$, influenced by weather conditions and

231   displaying significant fluctuations (Fig. 2d). From different seasons, the daily average of PAR in the

232   dry season (476.50 $\mu mol \cdot m^{-2} \cdot s^{-1}$) exceeded that of the rainy season (432.79 $\mu mol \cdot m^{-2} \cdot s^{-1}$). During

233   the dry season, the mean Ta was 23.04°C, while in the rainy season, it averaged 25.38°C. The

234   difference was small. Secondly, the highest and lowest values of Ta appear in May of the dry season.

235   The range of Ta and Ts was 8–34.52°C and 11.58–36.97°C, respectively. The seasonal variation

236   characteristics of the two were similar, but the Ts was significantly higher than the Ta, and the

237   change time lags behind the Ta (Fig. 2e). In terms of changes in Ws characteristics, the highest value

238   of Ws appeared in March, reaching 2.93 $m \cdot s^{-1}$, and the lowest value appeared in June, which was

239   0.57 $m \cdot s^{-1}$. The daily average Ws was the highest in February, which was 1.90 $m \cdot s^{-1}$, and the lowest

240   in August, which was 0.99 $m \cdot s^{-1}$. The Ws decreased significantly after mid-July (Fig. 2f). Finally, it

is particularly noteworthy that the annual P in the study area has been continuously decreasing in recent years (Fig. 3), especially in 2023, which recorded the lowest annual P since historical data has been recorded.
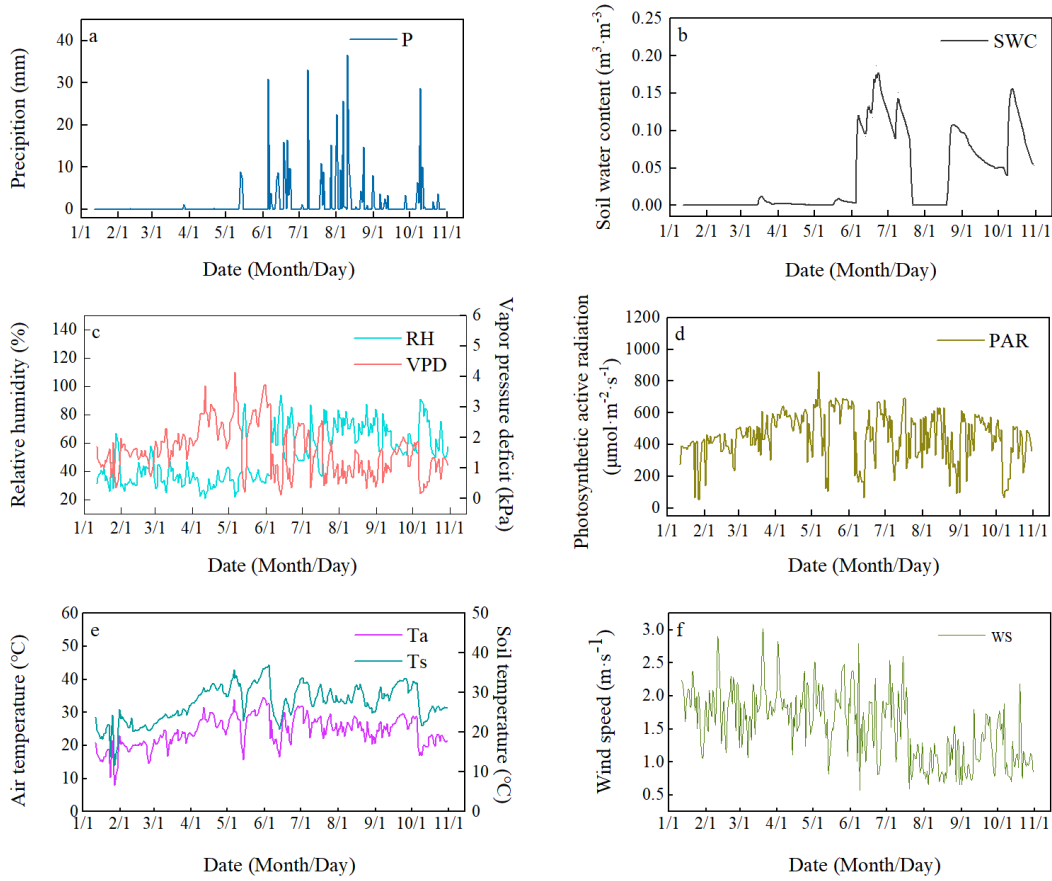

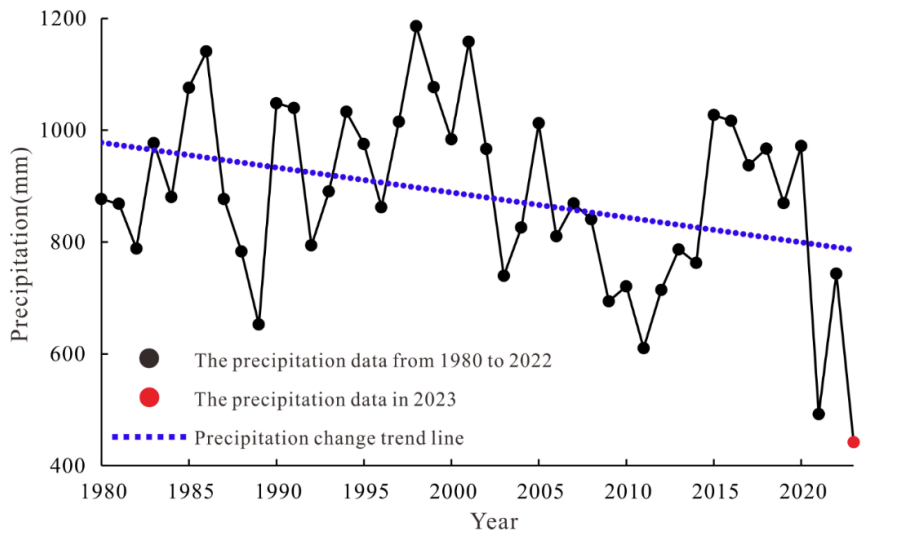Figure 2 The variation characteristics of environmental factors in the study area.

Figure 3 The precipitation changes in the study area from 1980 to 2023 (The precipitation data from 1980 to 2022 were collected from Yunnan Statistical Yearbook, and the precipitation data in 2023 were the measured data of Jinsha River Field Observation Station.).

3.2 Diurnal variation of CO_2 flux

The F_c was positive, indicating a C emission state, throughout the entire diurnal variation process in the dry season. The diurnal variation showed a 'W'-type bimodal curve (Fig. 4a) of decreasing → increasing → decreasing → increasing, that is, the F_c was lower in the morning and afternoon, and the F_c was higher in the nighttime and noon, especially in April and May when this diurnal variation pattern was most pronounced. The lowest F_c values appeared in the morning (8:00−10:00) of each month, which were 0.1178 $\mu mol \cdot m^{-2} \cdot s^{-1}$, 0.1148 $\mu mol \cdot m^{-2} \cdot s^{-1}$, and 0.1397 $\mu mol \cdot m^{-2} \cdot s^{-1}$, respectively. The highest F_c value appeared in the evening (19:20) in March, which was 0.2158 $\mu mol \cdot m^{-2} \cdot s^{-1}$. In April and May, it appeared in the evening (13:35). They were 0.1148 $\mu mol \cdot m^{-2} \cdot s^{-1}$ and 0.1397 $\mu mol \cdot m^{-2} \cdot s^{-1}$, respectively. During the dry season, the herbaceous plants in the study area were in a senescent state, and the grassland ecosystem was characterized solely by soil respiration. The study by Carey et al. (2016) found that in all non-desert biomes, soil respiration increases with rising soil temperature, however, beyond a certain threshold, the soil respiration rate decreases with further temperature increases. Therefore, we believe that the diurnal variation of F_c in the grassland of the JS dry hot valley during the dry season primarily relates to the diurnal variation of temperature. From night to morning, the temperature gradually decreased, leading to a reduction in soil respiration and a decrease in F_c. It was not until around 10:00 AM that the temperature began to rise, increasing in the intensity of soil respiration and a continuous rise in F_c, reaching its peak. Subsequently, the soil respiration rate decreased with further temperature increases, and after about 5:00 PM, as the temperature gradually declined, the limitation on soil respiration weakened, and carbon flux gradually increased again.

The diurnal variation of the F_c was characterized by a 'U'-shaped single-peak curve, which was stable at night and decreased first and then increased during the day (Fig. 4b), during the rainy season. At about 7:35 in the morning, with the increase of PAR intensity, the photosynthesis of the grassland ecosystem is continuously enhanced, and the F_c begins to become negative. At this time, the grassland ecosystem changes from C emission at night to C absorption, forming the source of CO_2 absorption and reaching the maximum peak of C absorption at 10:00−14:00. Until about 17:20, the F_c becomes positive again. The grassland ecosystem transitions into a state of C emission, releasing CO_2 into the atmosphere. During the rainy season, the SWC in the grassland was relatively high, and the increase in SWC had an inhibitory effect on the temperature sensitivity of soil respiration (Xiang et al., 2017). As a result, the F_c during the nighttime period remained relatively stable. The lowest F_c values appeared in the morning (10:00−12:00) from the diurnal variation of flux in various months, which were −1.4286 $\mu mol \cdot m^{-2} \cdot s^{-1}$, −1.3834 $\mu mol \cdot m^{-2} \cdot s^{-1}$, and −1.0278

284　μmol·m^{-2}·s^{-1}, respectively. The highest Fc values appeared in the evening (18:35–18:50), which

285　were 0.7584 μmol·m^{-2}·s^{-1}, 0.4959 μmol·m^{-2}·s^{-1} and 0.5715 μmol·m^{-2}·s^{-1}, respectively.
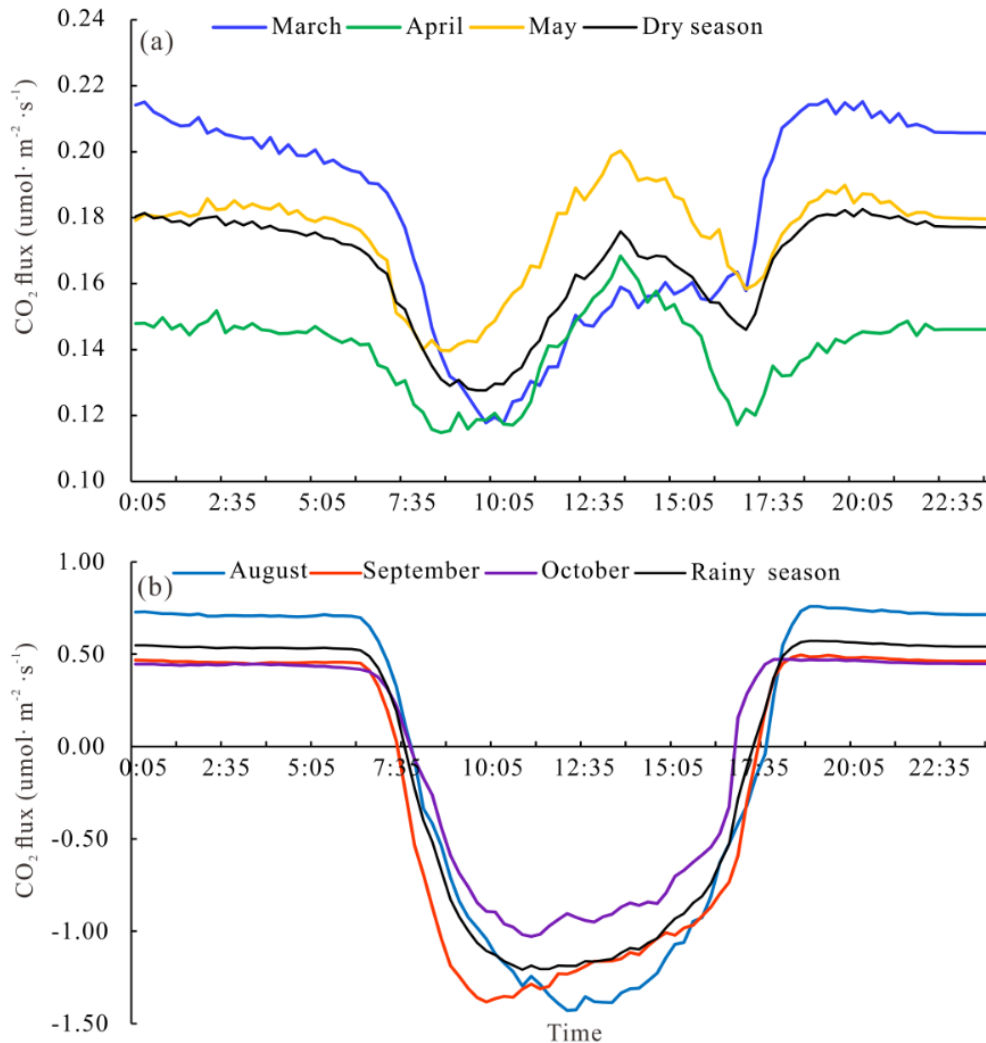
286

287　Figure 4 Diurnal variation characteristics of the Fc (a−dry season; b−rainy season).

288　3.3 Seasonal variation of CO$_2$ flux

289　　　From Fig.5, we can find that the seasonal variation of the Fc in the grassland ecosystem was

290　evident. In the dry season, the ecosystem experiences severe drought and water scarcity, leading to

291　poor growth of herbaceous plants, which is characterized by C emissions. The monthly cumulative

292　CO$_2$ emission fluxes were 18.64 g·m^{-2}, 15.96 g·m^{-2}, and 20.64 g·m^{-2}, respectively, displaying an

293　initial decline followed by a rise. The CO$_2$ emission flux was the highest in May. The ecosystem has

294　abundant P in the rainy season, the SWC is high, the herbaceous plants are in the growing season,

295　and the photosynthesis capacity is significant, so it is characterized by the C sink function. The

296　monthly cumulative CO$_2$ absorption fluxes were 6.42 g·m^{-2}, 24.41 g·m^{-2}, and 5.14 g·m^{-2},

297　respectively, displaying a rise initially followed by a decline, and the C absorption capacity in

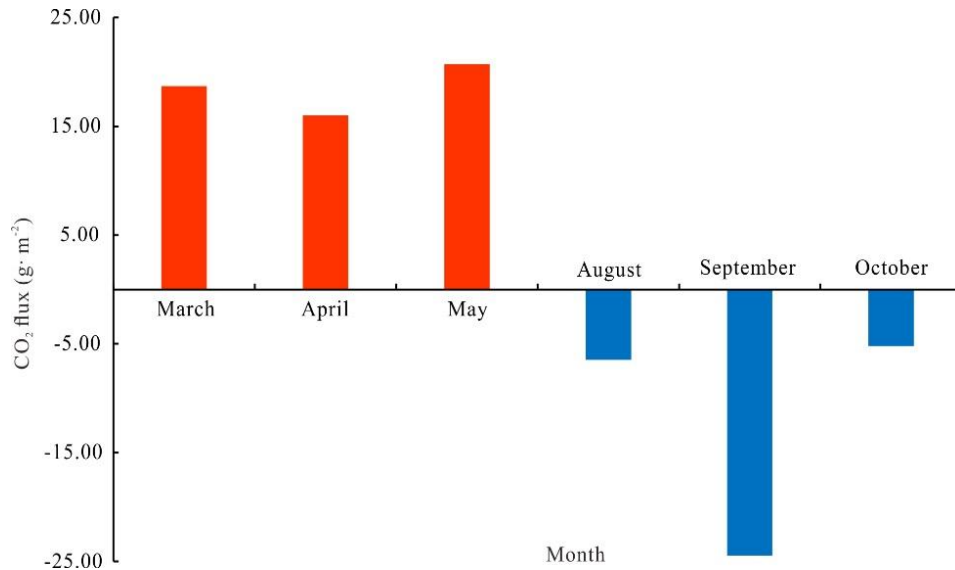298　September was the most significant.

Figure 5 Monthly variation characteristics of the F*c*.

The existing observation data were averaged and calculated respectively in this study, and they were used as the daily mean F*c* of the two seasons in the whole year. According to the days of the dry season (213 days) and the rainy season (152 days) in the whole year, the dry season, rainy season, and annual F*c* of the grassland ecosystem were calculated. The findings indicated that the mean daily F*c* was 0.1632 $\mu mol \cdot m^{-2} \cdot s^{-1}$, and the cumulative CO_2 emission was 1.3215 $t \cdot ha^{-1}$ in the dry season. The daily average F*c* was -0.1062 $\mu mol \cdot m^{-2} \cdot s^{-1}$, and the cumulative CO_2 uptake was 0.6137 $t \cdot ha^{-1}$ in the rainy season. From the annual scale, the cumulative F*c* of the grassland ecosystem was 0.7078 $t \cdot ha^{-1} \cdot a^{-1}$ (0.1926 t $C \cdot ha^{-1} \cdot a^{-1}$), making it a weak C source.

3.4 The relationship between CO_2 flux and environmental factors

3.4.1 Response of CO_2 flux to PAR

This study selected the F*c* data and the micrometeorological observation data corresponding to period and analyzed the mutual correlation between F*c* and environmental factors. The research area belongs to a typical semi-arid region, where vegetation growth and physiological processes are mainly regulated by temperature and moisture factors (Jiang et al., 2007; Fei et al., 2017a). Therefore, when analyzing the influencing factors of ecosystem CO_2 flux, we mainly selected environmental factors including P, SWC, Ts, Ta, RH, PAR, and VPD for Pearson analysis. No significant correlation between PAR and F*c* during the dry season was indicated by the results of the Pearson correlation analysis (R = 0.180, $P = 0.092$). Still, there was a strong negative correlation between PAR and F*c* during the rainy season (R = -0.578, $P < 0.01$), and this relationship was more obvious in Fig. 6a. As a key environmental factor driving plant photosynthesis, photosynthetically active radiation will directly affect the C absorption rate of grassland ecosystem and further affect the C budget pattern of the ecosystem. In the rainy season, the F*c* of the grassland ecosystem

12

decreased with the increase of PAR, and the C absorption capacity increased continuously, and the relationship between them could be expressed by formula (3). Secondly, when PAR was under 500 $\mu mol \cdot m^{-2} \cdot s^{-1}$ (Fig. 6b), the NEE of the ecosystem decreases rapidly with increasing PAR. At the same time, the distribution of NEE with PAR was relatively concentrated. However, when PAR was above 500$\mu mol \cdot m^{-2} \cdot s^{-1}$, the magnitude of the decrease in NEE with increasing PAR gradually decreases, and the distribution of NEE with PAR was relatively scattered, indicating that the F_c was also influenced by various other environmental factors present in the ecosystem when solar radiation is high. Once PAR reaches the light saturation point at 1523.64 $\mu mol \cdot m^{-2} \cdot s^{-1}$, the NEE of the ecosystem reached to its minimum, and the light response curve gradually begins to flatten. These research findings align with those of previous studies carried out in diverse grassland ecosystems (Zhao et al., 2007; Wang et al., 2015; Guo et al., 2022).
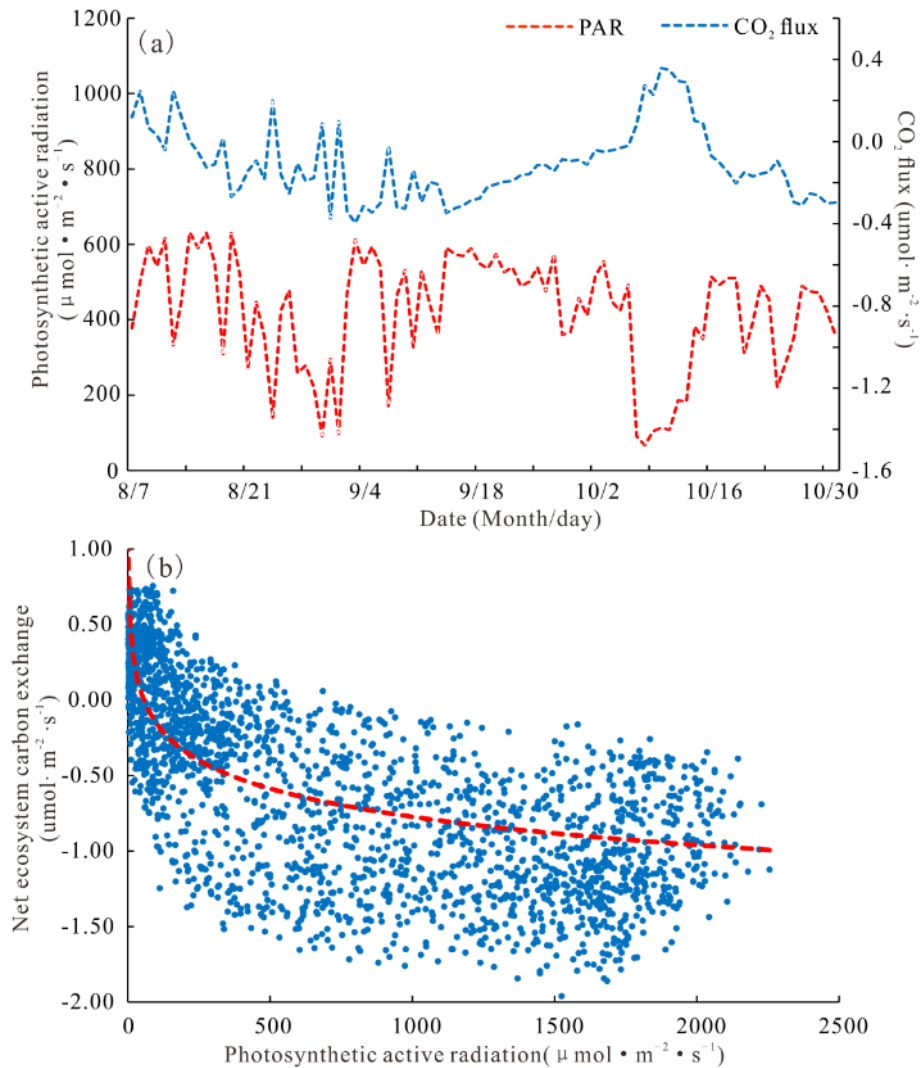

Figure 6 The correlation between PAR and F_c (a−the relationship between PAR and F_c in the rainy season; b−the response of F_c to PAR during daytime in the rainy season).

337 3.4.2 Relationship with other environmental factors

338   With no significant correlation with SWC (Fig. 7a and 7b) shown by the daily scale F_c of

339 grassland ecosystems in the various seasons, there was a moderate negative correlation with Ta and

340 Ts ($P<0.01$), a moderate positive correlation with P ($P<0.01$), and a strong positive correlation with

341 RH ($P<0.01$). The daily scale F_c in the dry season has a moderate negative correlation with VPD

342 ($P<0.01$), while the F_c in the rainy season shows a strong negative correlation with VPD ($P<0.01$).

343 Throughout varying seasons, the F_c increases with the increase of P and RH, as well as the decrease

344 of Ta, Ts, and VPD. Due to the small variations in SWC within the two seasons (Fig. 2b), therefore,

345 the impact of SWC on the diurnal fluctuation of the F_c was not significant. In general, the diurnal

346 variation of F_c in the dry season is mainly affected by RH, while the rainy season is mainly affected

347 by RH and VPD, and the influence of other environmental factors is generally weak.
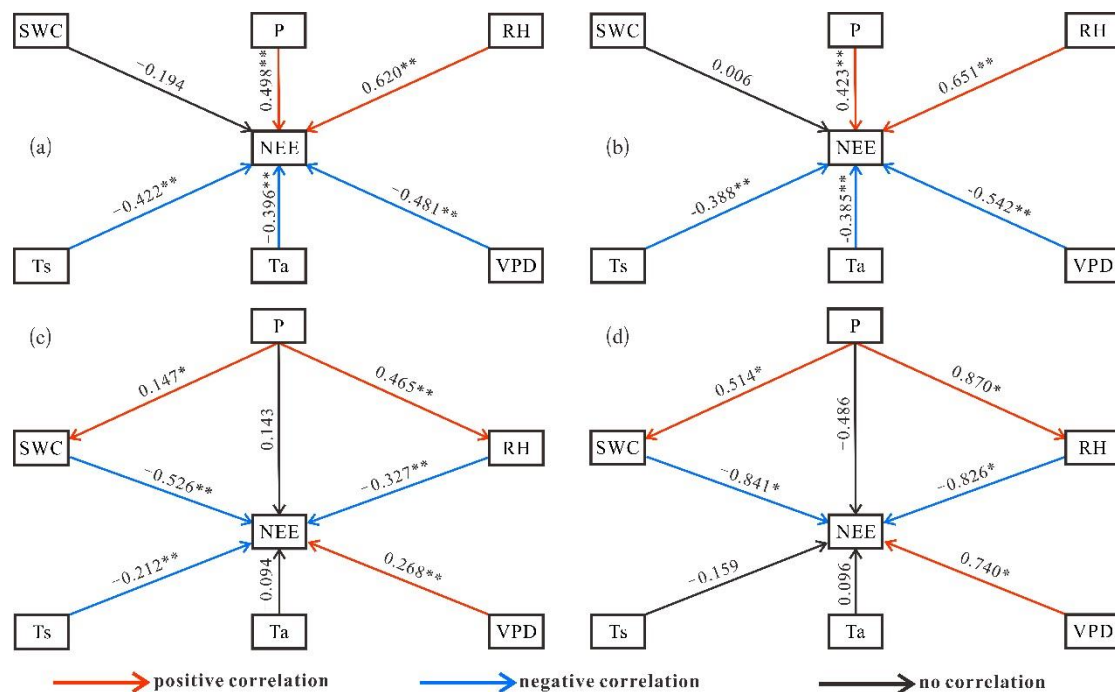

348 Figure 7 The Pearson correlation between F_c and environmental factors (a–daily scales of the dry season; b–daily

350 scales of the rainy season; c–annual daily scales; d–monthly scales, the ** is $P<0.01$; the * is $P<0.05$).

351   Throughout the year on a daily scale (Fig. 7c), the F_c showed no significant correlation with

352 Ta and P, a weak positive correlation with VPD ($P<0.01$), a weak negative correlation with Ts

353 ($P<0.01$), a moderate negative correlation with RH ($P<0.01$), and a strong negative correlation with

354 SWC ($P<0.01$). It is evident that as the time series extends, the physiological responses of

355 photosynthesis and respiration processes in the grassland ecosystem to specific environmental

356 factors have changed. As the VPD decreases, RH, SWC, and Ts increase and the F_c of the ecosystem

357 decreases gradually. Particularly, the impact of SWC was most significant, closely related to the

358 distinct climatic characteristics of wet and dry seasons in the study area. Under such climatic

14

conditions, the variation in SWC throughout the year becomes the dominant factor restricting regional vegetation growth and recovery (Jiang et al., 2007), significantly influencing the intra-annual variation of the F_c.

The study also found that at the monthly scale, the F_c showed no significant correlation with Ta, Ts, and P (Fig. 7d), but exhibited a strong negative correlation with SWC and RH ($P<0.05$), and a strong positive correlation with VPD ($P<0.05$). As the temporal scale increases, the environmental driving factors influencing the variation in F_c decrease, but the correlation significantly increases. This may be attributed to the short monthly time series of the observational data. In general, at the monthly scale, SWC, RH, and VPD emerge as the predominant factors influencing the variation in F_c within the ecosystem. Furthermore, the change in time scale will also affect the correlation between F_c and driving factors, aligning with the findings in the Heihe River Basin (Bai et al., 2022).

4 Discussion

4.1 CO_2 flux of grassland ecosystem

The herbs in the study area are mainly C_4 plants (Grace et al., 1995), which are called high-efficiency photosynthetic plants, and the C_4 plants exhibit higher efficiency in photosynthesis and resource utilization when compared to C_3 plants (Cui et al., 2021; Arslan et al., 2023; Xu et al., 2023). However, similar to other savanna ecosystems, the study area has been in a dry, high-temperature, and low-rainy climate for a long time. This extreme climatic condition makes the productivity of C_4 herbaceous plants only maintained at a medium level (Grace et al., 1995), therefore, the C sink capacity is relatively weak. The current study showed that within the grassland ecosystem situated in the JS dry hot valley, the daily maximum CO_2 uptake rate was recorded at only 1.4286 $\mu mol \cdot m^{-2} \cdot s^{-1}$, which stands notably lower in comparison to other grasslands found in arid and semi-arid regions (2.16 to 7.90 $\mu mol \cdot m^{-2} \cdot s^{-1}$), such as meadow steppe and desert steppe on the northern slope of Tianshan Mountains (Hu et al., 2018; Guo et al., 2022), Horqin sandy grassland (Niu et al., 2018), Tongyu semi-arid degraded grassland (Du et al., 2012), and Loess Plateau semi-arid grassland (Zhang et al., 2020).

Fei et al. (2017b) found that most savanna ecosystems globally demonstrate C sequestration features, with only a few exhibiting characteristics of C emissions, with the NEE varying from around -3.87 to 1.28 t $C \cdot ha^{-1} \cdot a^{-1}$. Among them, the savanna ecosystem with C source characteristics is mainly grassland savanna and semi-arid savanna, especially the grassland savanna has the largest annual C emissions (Archibald et al., 2009; Hutley et al., 2005; Quansah et al., 2015), which is similar to the results of this study. In the arid/semi-arid regions of China, the NEE of different

391 grassland ecosystems varies between –3.08 to 0.96 t C·ha^{-1}·a^{-1} (Du et al., 2012; Niu et al., 2018;

392 Chen et al., 2019; Zhang et al., 2020; Bai et al., 2022). We found that most grasslands act as C sinks,

393 with only a few, such as the Horqin sandy grassland (Niu et al., 2018; Chen et al., 2019), exhibiting

394 C source characteristics, and the C emissions (0.91 to 0.96 t C·ha^{-1}·a^{-1}) is higher than those of the

395 grasslands in the JS dry-hot valley. Consistent with findings from other savanna ecosystems (Grace

396 et al., 1995; Miranda et al., 1997; Fei et al., 2017a), the special hydrothermal conditions make the

397 vegetation growth of the grassland in the study area exhibit pronounced seasonal characteristics and

398 affect the change of Fc. In the season of drought and water shortage, the herbs' growth is poor, and

399 the ecosystem mainly emits C, showing a C source characteristic. During the rainy season, the

400 vegetation enters the peak period of growth, with strong C fixation ability, and the ecosystem mainly

401 absorbs CO_2, showing a C sink function. Overall, the grassland ecosystems in the study area

402 predominantly exhibit C emissions, albeit at relatively low levels, demonstrating a C-neutral

403 attribute. The Fc characteristics are the same as those of the Sumbrugu Aguusi savanna grassland in

404 Sudan (Quansah et al., 2015), Kruger Park semi-arid savanna in South Africa (Archibald et al.,

405 2009), and Virginia Park semi-arid savanna in Australia (Hutley et al., 2005).

406 Through comparative analysis, we found that most of the grasslands in the savanna ecosystem

407 and arid and semi-arid areas are dominated by C sinks. The reason for the C emission status of

408 grassland in this study may be attributed to the continuous reduction of rainfall in the study area in

409 recent years (Fig. 3). Under this extremely dry and rainless climate condition, the C sequestration

410 capacity of herbaceous plants with low productivity is significantly reduced. In the case of

411 continuous reduction of rainfall in the future, the C emissions from grassland ecosystems in the

412 study area may continue to rise. At the same time, the study area is a unique heat island habitat in

413 the global temperate zone. Under the climate scenario of continuous warming and decreasing

414 precipitation in the future, the vegetation community structure in some temperate regions will shift

415 to the savanna vegetation community (Yang and Chang, 2007; Jing et al., 2024). With the extension

416 of drought and high temperature, grassland ecosystems in these areas may change from C sinks to

417 C sources, which is extremely important for the C balance of global terrestrial ecosystems.

418 ## 4.2 Effects of environmental factors on CO_2 flux

419 ### 4.2.1 Temperature factor

420 As a crucial environmental factor influencing the Fc of ecosystems, temperature mainly affects

421 the Fc of terrestrial ecosystems by regulating biological activities such as photosynthesis and

422 respiration (Woodwell et al., 1983; Pan et al., 2020; Johnston et al., 2021; Chen et al., 2023),

423 especially for grassland ecosystems, several prior studies have validated that temperature serves as

the primary driving force controlling the variation in Fc. Nevertheless, owing to variations in climate and environmental conditions, the regulatory impact of temperature fluctuations on the Fc differs significantly across various types of grassland ecosystems. Compared with temperate grassland and semi-arid grassland, the warming effect has the most significant impact on the Fc of frigid grasslands worldwide. However, in semi-arid grassland ecosystems, the effect of warming is not significant (Wang et al., 2019). The rise in temperature (both annual average temperature and annual average soil temperature) reduced the Fc of temperate grasslands in China, while the effect on alpine grasslands was the opposite (Liu et al., 2024). In the Inner Mongolia Plateau, with the increase of temperature, the NEE of the grassland ecosystem will increase (Liu et al., 2018), while the change of Qinghai–Tibet Plateau, compared with it, is very small, and there is no correlation between Fc and temperature change in the Inner Mongolia grassland during the drought period (Hao et al., 2006). Ta and Ts exhibit a negative correlation with the Fc at different seasonal daily scales in the grassland ecosystem in the dry-hot valley of JS, similar to the control mechanisms seen in other arid and semi-arid grasslands (Li et al., 2015; Niu et al., 2018; Chen et al., 2019). As the time series extends and the temporal scale increases, the impact of Ta and Ts on the fluctuations in the Fc in the grassland of the study region continues to weaken, which is related to the small differences in Ta and Ts within different time scales in the study area. That is, the small temperature difference leads to the distribution change of the Fc in time is not sensitive to temperature fluctuation, which is the same as the characteristics of the savanna ecosystem in YJ (Fei et al., 2017a). This phenomenon is also common in other arid regions (Wang et al., 2021).

4.2.2 Water factor

Previous studies have pointed out that a potential limiting factor affecting C uptake in terrestrial ecosystems is soil moisture, which can diminish NPP through water stress in ecosystems, leading to vegetation death (Green et al., 2019). Simultaneously, soil moisture may exacerbate extreme climatic conditions through the intricate interaction between the land and the atmosphere. Particularly in arid regions characterized by scarce water resources, there exists a significant interaction between soil moisture and vegetation. Hence, in terms of C and water fluxes affecting dryland ecosystems, SWC is a more important ecosystem control factor than Ta (Zhang et al., 2012; Zou et al., 2016; Fei et al., 2017a; Tarin et al., 2020; Kannenberg et al., 2024). For instance, in the herbs growth season of the Qinghai–Tibet Plateau, regions with plentiful precipitation in the east and southeast primarily regulate C absorption capacity through temperature. Conversely, SWC emerges as the principal determinant of C sequestration capability in the arid and water shortage western region (Wang et al., 2021). Simultaneously, the SWC emerges also as the predominant

factor influencing the diurnal fluctuations of NEE in grassland in the semi-arid regions of northern China (Zhao et al., 2020). In the sandy grasslands of Horqin, the NEE during the plant growth season increases with the rise in SWC, while it decreases during the non-growth season (Chen et al., 2019).

The research area is a classic dryland ecosystem characterized by scarce and concentrated precipitation. The driving effect of water on the ecosystem is obvious. Plant physiology is greatly affected by water stress. To further assess the impact of SWC in the dry-hot valley of the JS on NEE, we divided the grassland SWC into three levels: low SWC ($0 \ m^3 \cdot m^{-3} \leq SWC \leq 0.05 \ m^3 \cdot m^{-3}$), moderate SWC ($0.05 \ m^3 \cdot m^{-3} < SWC \leq 0.10 \ m^3 \cdot m^{-3}$), and high SWC ($0.10 \ m^3 \cdot m^{-3} < SWC$), corresponding to dry, intermediate, and wet periods, respectively. We then analyzed the relationship between SWC and NEE during these different periods (Fig. 8). During the dry period, SWC showed a weak negative correlation with NEE ($R = -0.297$, $P < 0.01$). In the intermediate period, there was a strong negative correlation between SWC and NEE ($R = -0.500$, $P < 0.01$). In the wet period, SWC exhibited a strong positive correlation with NEE ($R = 0.661$, $P < 0.01$). The results indicate that within an appropriate range of SWC, an increase in SWC can effectively enhance the C sink capacity of the grasslands in the dry-hot valley of the JS. However, when SWC exceeds a certain threshold, an increase in SWC may inhibit the C absorption capacity of the grasslands. As found by Davidson et al. (1998) and Taylor et al. (2017), net ecosystem productivity increases with rising SWC in dry environments, reaching a maximum under optimal conditions, and then decreases in waterlogged environments. Our research results support this ecological process well.
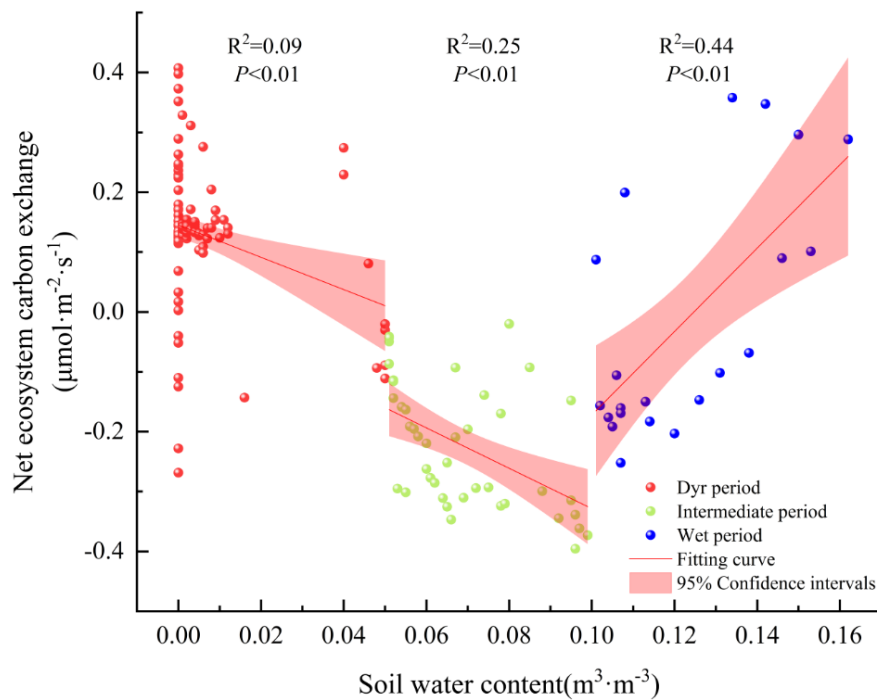

Figure 8 Relationship between NEE and SWC.

478   In arid ecosystem, alterations in the P significantly affect plants and soil, especially the

479   grassland ecosystem has the greatest response to the change of the P. The effectiveness of water

480   dictates plant growth and the release and absorption of CO_2. Therefore, prior research has indicated

481   that the Fc of grasslands in arid regions exhibits greater sensitivity to variations in the P (Knapp et

482   al., 2002; Niu et al., 2007; Weltzin et al., 2003; Zhang et al., 2020). An increase in the P led to a

483   delay in the peak of gross primary productivity in vegetation growth stage of the Inner Mongolia

484   desert steppe, enhancing the ecosystem's Fc (Li et al., 2017; Zhang et al., 2019). The decrease of

485   the P significantly reduced the soil respiration in the early and middle vegetation growth season of

486   Horqin sandy grassland (Wang et al., 2023). The P of Xilinhot grassland changed the Fc in the

487   vegetation growth season mainly by affecting SWC (Wang et al., 2015). High water levels (annual

488   average precipitation and soil moisture) have continuously increased the Fc of temperate grasslands

489   and alpine grasslands in the Mongolian Plateau, Loess Plateau, and Qinghai–Tibet Plateau (Liu et

490   al., 2024).

491   Changes in hydrological conditions such as the P and SWC can significantly affect the water

492   balance characteristics and water redistribution of the savanna ecosystems due to the arid and hot

493   climate environment characteristics, thereby altering the ecological system structure and vegetation

494   community composition of woody and herbaceous plants coexisting (Yu et al., 2015; Lee et al.,

495   2018; Jin et al., 2019; Zhang et al., 2019; Hoffmann, 2023; Mattos et al., 2023), thereby affecting

496   vegetation productivity (Jin et al., 2018), ecological water use efficiency (Yu et al., 2015; Lee et al.,

497   2018; Mattos et al., 2023), plant diversity (He, et al., 2024), and Fc (Fei et al., 2017a). As far as the

498   grassland ecosystem in the dry-hot valley of JS is concerned, the P shows a positive correlation with

499   the Fc at different seasonal daily scales, with no significant relationship observed with the Fc

500   variation on the daily and monthly scales throughout the year. However, the variation in P

501   significantly affects the regional SWC and RH (Fig. 7c and 7d). Therefore, we suggest that the

502   impact mechanism of the P on the Fc in the JS dry-hot valley grassland ecosystem may be similar

503   to that of the Xilinhot grassland ecosystem, where the P mainly controls vegetation growth by

504   affecting SWC and RH, thereby indirectly influencing the Fc in the grassland ecosystem.

505   4.2.3 Relative humidity and vapor pressure deficit factor

506   The arid/semi-arid grassland ecosystem is short of water resources, the soil nutrients are

507   relatively poor, and the ecosystem is fragile and sensitive. Especially with the change in global

508   climate, RH has become a key limiting factor restricting its sustainable development (Wang et al.,

509   2023). As an important measure of atmospheric dryness, the fluctuation of VPD is controlled by RH

510   and has a high correlation with other important driving factors of ecosystem productivity, such as

Ta and SWC, which is a key climate regulation factor affecting ecosystem photosynthesis and transpiration. Multiple studies have shown that when RH decreases, vegetation stomata will be closed due to an increase in VPD, thereby preventing excessive water loss (Williams et al., 2013; Novick et al., 2016; Sulman et al., 2016; Hsu et al., 2021), leading to a decrease in the photosynthetic rate of leaves and canopies, thereby inhibiting photosynthesis (McDowell et al., 2015; Sulman et al., 2016; Yuan et al., 2019), reducing vegetation productivity and hindering vegetation growth. Therefore, there is a mainly negative correlation between the intensity of plant photosynthesis and VPD. Zhong et al. (2023) discovered that excluding the influences of Ta and soil moisture on vegetation productivity, VPD negatively impacts vegetation productivity in the majority of Northern Hemisphere regions. Globally, studies have also shown that increased VPD reduces global vegetation growth and offsets the beneficial impacts of CO_2 fertilization (Yuan et al., 2019). Simultaneously, the interannual variation of VPD shows a significant negative correlation with net ecosystem productivity and affects the interannual variation of atmospheric CO_2 growth rate (He et al., 2022). Because of variations in climatic conditions and the synergistic effects of multiple environmental factors, the response mechanisms of the Fc in different grassland ecosystems to changes in VPD and RH are also varied. For instance, in the savanna ecosystem of YJ, the Fc shows a negative correlation with VPD (Fei et al., 2017a). Wang et al. (2021) found through a study on the spatial variation of Fc of 10 distinct grassland types that a positive correlation exists between VPD and NEE in the Qinghai–Tibet Plateau. In the arid grasslands of the Heihe River Basin (Bai et al., 2022), the Fc is positively correlated with VPD and RH. The Fc at the daily scale exhibits a positive correlation with RH and a negative correlation with VPD during different seasons in the study area. Taking into account the seasonal changes in different environmental factors (Fig. 2c), during the dry season, the RH was low, and VPD was high. The ecosystem exhibits a C emission state, while the opposite is observed during the rainy season. Generally, the reduction in RH and the increase in VPD will inhibit the ecosystem's C absorption capacity.

5 Conclusions

This study quantitatively analyzed the Fc variations and their relationships with environmental factors in the grassland ecosystem of the dry-hot valley of JS, enriching the theoretical understanding of key C cycling processes in the savanna ecosystem in China. Nonetheless, the lack of long-term observational data on Fc in our study precludes a more thorough examination of the inter-annual variation characteristics of the Fc. Secondly, the study did not effectively monitor the dynamic characteristics of soil respiration, which made it impossible to accurately calculate the

ecosystem's GPP. Furthermore, we only observed and studied the changes in F*c* of the grassland ecosystem, while the savanna ecosystem has a vegetation community structure with two levels of shrub and grass. Therefore, our forthcoming research will emphasize the extended observation of the F*c* changes in the savanna ecosystem with a complete vegetation community structure, especially the use of eddy covariance methods to expand the scope of ecosystem observation and reduce the uncertainty of measurement samples, so as to better clarify the C budget pattern of the ecosystem. Through this research, we have arrived at the following findings:

(1) As a result of environmental factors, the F*c* of the grassland ecosystem in the JS dry-hot valley exhibited significant temporal variations. During the dry season, the grassland functioned as a C source, with the daily variation of F*c* showing a 'W'-shaped bimodal curve. In contrast, during the rainy season, the grassland functioned as a C sinks, with the daily variation of F*c* displaying a 'U'-shaped unimodal curve.

(2) The F*c* of grasslands during the dry season was primarily influenced by RH. During the rainy season, F*c* was significantly affected not only by PAR but also by SWC, RH, and VPD. Overall, SWC, RH, and VPD were the primary environmental factors influencing grassland F*c*. Particularly when SWC was within an optimal range, an increase in SWC can effectively enhance the C absorption capacity of the grassland. However, when SWC was in a wet period, an increase in SWC will lead to a rise in the ecosystem's NEE.

(3) The grassland in the JS dry-hot valley was a weak C source, which was closely related to the continuous reduction in precipitation in recent years. As precipitation continues to decline, the C sequestration capacity of herbaceous plants will significantly decrease, resulting in increased CO_2 emissions from the grasslands in the study area. Under a future climate scenario of continuous high temperatures and drought, the plant community structure in some temperate regions may shift to savanna, and the grasslands in these regions may shift from being C sinks to C sources, thereby impacting the global C balance.

Data availability

The CO_2 flux data and environmental data used to support the findings of this study were available from the corresponding author upon request. The administrative boundary data (DOI:10.12078/2023010101; DOI:10.12078/2023010103) and river data (DOI:10.12078/2018060101) were downloaded from the RESDC from the Chinese Academy of Sciences (https://www.resdc.cn/Default.aspx).

Author contributions

587

References

589   Archibald, S.A., Kirton, A., van der Merwe, M.R., Scholes, R.J., Williams, C.A., Hanan, N.: Drivers
590   of inter-annual variability in net ecosystem exchange in a semi-arid savanna ecosystem, South
591   Africa, Biogeosci, 6, 251–266, 2009.

592   Ago, E.E., Agbossou, E.K., Galle, S., Cohard, J.M., Heinesch, B., Aubinet, M.: Long term
593   observations of carbon dioxide exchange over cultivated savanna under a Sudanian climate in
594   Benin   (West   Africa),   Agric.   For.   Meteorol,   197,   13–25,
595   https://doi.org/10.1016/j.agrformet.2014.06.005, 2014.

596   Arslan, A.M., Wang, X., Liu, B.Y., Xu, Y.N., Li, L., Gong, X.Y.: Photosynthetic resource-use
597   efficiency trade-offs triggered by vapour pressure deficit and nitrogen supply in a C_4 species,
598   Plant Physiol. Biochem, 197, 107666, https://doi.org/10.1016/j.plaphy.2023.107666, 2023.

599   Bousquet, P., Ciais, P., Miller, J.B., Dlugokencky, E.J., Hauglustaine, D.A., Prigent, C., White, J.:
600   Contribution of anthropogenic and natural sources to atmospheric methane variability, Nature,
601   443, 439–443, https://doi.org/10.1038/nature05132, 2006.

602   Beringer, J., Hutley, L.B., Tapper, N.J., Cernusak, L.A.: Savanna fires and their impact on net
603   ecosystem productivity in North Australia, Global Change Biol, 13, 990–1004,
604   https://doi.org/10.1111/j.1365-2486.2007.01334.x, 2007.

605   Brümmer, C., Falk, U., Papen, H., Szarzynski, J., Wassmann, R., Brüggemann, N.: Diurnal, seasonal,
606   and interannual variation in carbon dioxide and energy exchange in shrub savanna in Burkina
607   Faso   (West   Africa),   J.   Geophys.   Res.:   Biogeosci,   113,   https://doi.org/Artn
608   G0203010.1029/2007jg000583, 2008.

609   Bai, Y.F., Cotrufo, M.F.: Grassland soil carbon sequestration: current understanding, challenges, and
610   solutions, Science, 377, 603‑608, https://doi.org/10.1126/science.abo2380, 2022.

611   Bai, X.J., Wang, X.F., Liu, X.H., Zhou, X.Q.: Dynamics and driving factors of carbon fluxes in
612   wetland，cropland and grassland ecosystems in Heihe river basin, Remote Sens, Technol. Appl,
613   37, 94‑107, https://doi.org/10.11873/j.issn.1004-0323.2022.1.0094, 2022.

614   Bai, X.Y., Zhang, S.R., Li, C.J., Xiong, L., Song, F.J., Du, C.C., Li, M.H., Luo, Q., Xue, Y.Y., Wang,

S.J.: A carbon-neutrality-capacity index for evaluating carbon sink contributions, Environ. Sci. Ecotechnol., 15, 100237, https://doi.org/10.1016/j.ese.2023.100237, 2023.

Bureau of Statistics of Yunnan Province. Yunnan Statistical Yearbook; China Statistics Press: Beijing, China, 2023.

Campbell, G.S., Norman, J.M.: An introduction to environmental biophysics, Springer Sci, Business Media, 2012.

Cleverly, J. Boulain, N., Villalobos-Vega, R., Grant, N., Faux, R., Wood, C., Cook, P.G., Yu, Q., Leigh, A., Eamus, D.: Dynamics of component carbon fluxes in a semi-arid Acacia woodland, central Australia, J. Geophys. Res.: Biogeosci, 118, 1168–1185, https://doi.org/10.1002/jgrg.20101, 2013.

Carey, C.J., Tang, J.W., Templer, P.H., Kroeger, K.D., Crowther, T.W., Burton, A.J., Dukes, J.S., Emmett, B., Frey, S.D., Heskel, M.A., Jiang, L.F., Machmuller, M.B., Mohan, J., Panetta, A.M., Reich, P.B., Reinsch, S., Wang, X., Allison, S.D., Bamminger, C., Bridgham, S., Collins, S.L., de Dato, G., Eddy, W.C., Enquist, B.J., Estiarte, M., Harte, J., Henderson, A., Johnson, B.R., Larsen, K.S., Luo, Y.Q., Marhan, S., Melillo, J.M., Peñuelas, J., Pfeifer-Meister, L., Poll, C., Rastetter, E., Reinmann, A.B., Reynolds, L.L., Schmidt, I.K., Shaver, G.R., Strong, A.L., Suseela, V., Tietema, A.: Temperature response of soil respiration largely unaltered with experimental warming, PNAS, 113, 13797−13802, https://doi.org/10.1073/pnas.1605365113, 2016.

Chen, Y.P., Niu, Y.Y., Li, W., Li, Y.Q., Gong, X.W., Wang, X.Y.: Characteristics of carbon flux in sandy grassland ecosystem under natural restoration in Horqin sandy land, Plateau Meteorol, 38, 650–659, https://doi.org/10.7522/.issn.1000-0534.2018.00133, 2019.

Cui, H.C.: Challenges and approaches to crop improvement through C_3-to-C_4 engineering, Front. Plant Sci, 12, 715391, https://doi.org/10.3389/fpls.2021.715391, 2012.

Chen, W.N., Wang, S., Wang, J.S., Xia, J.Y., Luo, Y.Q., Yu, G.R., Niu, S.L.: Evidence for widespread thermal optimality of ecosystem respiration, Nat. Ecol. Evol, 7, 1379–1387, https://doi.org/10.1038/s41559-023-02121-w, 2023.

Davidson, E.A., Belk, E., Boone, R.D.: Soil water content and temperature as independent or confounded factors controlling soil respiration in a temperate mixed hardwood forest, Glob. Chang. Biol. 4, 217–227 , https://doi.org/ 10.1046/j.1365-2486.1998.00128.x, 1998.

Du, Q., Liu, H.Z., Feng, J.W., Wang, L., Huang, J.P., Zhang, W., Bernhofer, C.: Carbon dioxide exchange processes over the grassland ecosystems in semiarid areas of China, Sci. China, Ser. D Earth Sci, 42, 711−722, https://doi.org/10.1007/s11430-011-4283-1, 2012.

Dobson, A., Hopcraft, G., Mduma, S., Ogutu, J.O., Fryxell, J., Anderson, M., Archibald, S., Lehmann, C., Poole, J., Caro, T., Mulder, M.B., Holt, R.D., Berger, J., Rubenstein, D.I., Kahumbu, P., Chidumayo, E.N., Milner-Gulland, E.J., Schluter, D., Otto, S., Balmford, A., Wilcove, D., Pimm, S., Veldman, J.W., Olff, H., Noss, R., Holdo, R., Beale, C., Hempson, G., Kiwango, Y., Lindenmayer, D., Bond, W., Ritchie M., Sinclair, A.R.E.: Savannas are vital but overlooked carbon sinks, Science, 375, 392, https://doi.org/10.1126/science.abn4482, 2022.

Deng, Y.: The boundary definition and studyon the land use/cover change and landscape pattern of the dry-hot valley in Hengduan Mountains, Yunnan University, https://doi.org/ 10.27456/d.cnki.gyndu.2022.000408, 2022.

Eamus, D., Hutley, L.B., O'Grady, A.P.: Daily and seasonal patterns of carbon and water fluxes above a north Australian savanna, Tree Physiol, 21, 977−988, 2001.

Fei, X.H., Song, Q.H., Zhang, Y.P., Liu, Y.T., Sha, L.Q., Yu, G.R., Zhang, L.M., Duan, C.Q., Deng, Y., Wu, C.S., Lu, Z.Y., Luo, K., Chen, A.G., Xu, K., Liu, W.W., Huang, H., Jin, Y.Q., Zhou, R.W., Li, J., Lin, Y.X., Zhou, L.G., Fu, Y., Bai, X.L., Tang, X.H., Gao, J.B., Zhou, W.J., Grace, J.: Carbon exchanges and their responses to temperature and precipitation in forest ecosystems in Yunnan, Southwest China, Sci. Total Environ, 616–617, 824–840, https://doi.org/10.1016/j.scitotenv.2017.10.239, 2017a.

Fei, X.H., Jin, Y.Q., Zhang, Y.P., Sha, L.Q., Liu, Y.T., Song, Q.H., Zhou, W.J., Liang, N.S., Yu, G.R., Zhang, L.M., Zhou, R.W., Li, J., Zhang, S.B., Li, P.G.: Eddy covariance and biometric measurements show that a savanna ecosystem in Southwest China is a carbon sink, Sci Rep, 7, 41025, https://doi.org/10.1038/srep41025, 2017b.

Grace, J., Lloyd, J., McIntyre, J., Miranda, A.C., Meir, P., Miranda, H., Moncrieff, J.M., Massheder, J., Wright, I.R., Gash, J.: Fluxes of carbon dioxide and water vapour over an undisturbed tropical forest in south-west Amazonia, Global Change Biol, 1, 1–12, https://doi.org/10.1111/j.1365-2486.1995.tb00001.x, 1995.

Grace, J., José, J. S., Meir, P., Miranda, H. S., Montes, R.A.: Productivity and carbon fluxes of tropical savannas, J. Biogeogr, 33, 387–400, https://doi.org/10.1111/j.1365-2699.2005.01448.x., 2006.

Green, J. K., Seneviratne, S. I., Berg, A. M., Findell, K. L., Hagemann, S., Lawrence, D. M., Gentine, P.: Large influence of soil moisture on long-term terrestrial carbon uptake, Nature, 565, 476–479, https://doi:10.1038/s41586-018-0848-x, 2019.

Guo, W.Z., Jing, C.Q., Deng, X.J., Chen, C., Zhao, W.K., Hou, Z.X., Wang, G.X.: Variations in carbon flux and factors influencing it on the northern slopes of the Tianshan Mountains, Acta Prataculturae Sin, 31, 1−12. https://doi.org/10.11686/cyxb2021137, 2022.

He, Y.B., Lu, P.Z., Zhu, T.: Causes for the formation of dry-hot valleys in Hengduan Mountain-Yunnan plateau, Resour. Sci, 22, 69–72, https://www.resci.cn/CN/Y2000/V22/I5/69, 2000.

Houghton, R.A.: Counting terrestrial sources and sinks of carbon, Clim. Change, 48, 525−534, https://doi.org/10.1023/A:1005658316062, 2001.

Hutley, L.B., Leuning, R., Beringer, J., Cleugh, H.A.: The utility of the eddy covariance techniques as a tool in carbon accounting: tropical savanna as a case study, Aust. J. Bot, 53, 663–675, https://doi.org/10.1071/Bt04147, 2005.

Hao, Y.B., Wang, Y.F., Sun, X.M., Huang, X.Z., Cui, X.Y., Niu, H.S., Zhang, Y.H., Yu, G.R.: Seasonal variation in carbon exchange and its ecological analysis over Leymus chinensis steppe in Inner Mongolia, Sci. China, Ser. D Earth Sci, 49, 186–195, https://doi.org/10.1007/s11430-006-8186-5, 2006.

Harmon, T.C., Dierick, D., Trahan, N., Allen, M.F., Rundel, P.W., Oberbauer, S.F., Schwendenmann, L., Zelikova, T.J.: Low−cost soil CO_2 efflux and point concentration sensing systems for terrestrial ecology applications, Methods Ecol. Evol, 6, 1358–1362, https://doi.org/10.1111/2041-210X.12426, 2015.

Hu, Y., Zhu, X.P., Jia, H.T., Han, D.L., Hu, B.A., Li, D.P.: Effects of fencing on ecosystem crabon exchange at meadow steppe in the northern slop oh the Tianshan Mountains, Chinese J. Plant Eco, 42, 372–381, https://doi.org/10.17521/cjpe.2016.0049, 2018.

Hsu, P.K., Takahashi, Y., Merilo, E., Costa, A., Zhang, L., Kernig, K., Lee, K.H., Schroeder, J.I.: Raf-like kinases and receptor-like (pseudo)kinase GHR1 are required for stomatal vapor pressure difference response, PNAS, 118, e2107280118, https://doi.org/10.1073/pnas.21072801,

703   2021.

704   He, B., Chen, C., Lin, S.R., Yuan, W.P., Chen, H.W., Chen, D.L., Zhang, Y.F., Guo, L.L., Zhao, X.,

705   Liu, X.B., Piao, S.L., Zhong, Z.Q., Wang, R., Tang, R.: Worldwide impacts of atmospheric vapor

706   pressure deficit on the interannual variability of terrestrial carbon sinks, Natl. Sci. Rev, 9,

707   nwab150, https://doi.org/10.1093/nsr/nwab150, 2022.

708   Hoffmann, W.A.: Seasonal flooding shapes forest–savanna transitions, PNAS, 120, e2312279120,

709   https://doi.org/10.1073/pnas.2312279120, 2023.

710   He, G.X., Shi, Z.T., Fang, H.D., Shi, L.T., Wang, Y.D., Yang, H.Z., Yan, B.G., Yang, C.L., Yu, J.L.,

711   Liang, Q.L., Zhao, L., Jiang, Q.: Climate and soil stressed elevation patterns of plant species to

712   determine the aboveground biomass distributions in a valley-type Savanna, Front. Plant Sci, 15,

713   1324841, https://doi.org/10.3389/fpls.2024.1324841, 2024.

714   Jin, Z.Z., Ou, X.K., Zhou, Y.: The general situation of natural vegetation in dry-hot river valley of

715   Yuanmou, Yunnan Province, Chin. J. Plant Ecol, 11, 308−317, 1987.

716   Jiang, J.M., Fei, S.M., He, Y.P., Zhang, F., Kong, Q.H.: Study on vegetation restoration in dry-hot

717   valleys of the Jinsha River, J. Southwest For. Univ, 27, 11–15,

718   https://doi.org/10.11929/j.issn.2095-1914.2007.06.003, 2007.

719   Jin, Y.Q., Li, J., Liu, C.G., Liu, Y.T., Zhang, Y.P., Song, Q.H., Sha, L.Q., Chen, A.G., Yang, D.X.,

720   Li, P.G.: Response of net primary productivity to precipitation exclusion in a savanna ecosystem,

721   For. Ecol. Manage, 29, 69−76, https://doi.org/10.1016/j.foreco.2018.07.007, 2018.

722   Jin, Y.Q., Li, J., Liu, C.G., Liu, Y.T., Zhang, Y.P., Song, Q.H., Sha, L.Q., Balasubramanian, D., Chen,

723   A.G., Yang, D.X., Li, P.G.: Precipitation reduction alters herbaceous community structure and

724   composition in a savanna, J. Veg. Sci, 30, 821–831, https://doi.org/10.1111/jvs.12766, 2019.

725   Johnston, A.S.A., Meade, A., Ardö, J., Arriga, N., Black, A., Blanken, P.D., Bonalo, D., Brümmer,

726   C., Cescatti, A., Dušeko, J., Grafo, A., Gioli, B., Godedo, I., Gougho, C.M., Ikawa, H., Jassalo,

727   R., Kobayashi, H., Magliulo, V., Mancao, G., Montagnani, L., Moyano, F.E., Olesen, J.E., Sachs,

728   T., Shao, C.L., Tagesson, T., Wohlfahrt, G., Wolfo, S., Woodgate, W., Varlagin, A., Venditti, C.:

729   Temperature thresholds of ecosystem respiration at a global scale, Nat. Ecol. Evol, 5, 487–494,

730   https://doi.org/10.1038/s41559-021-01398-z, 2021.

731   Jiang, Q.Q., He, J.J., Li, Y.R., Yang, X.Y., Peng, Y., Wang, H., Yu, F., Wu, J., Gong, S.L., Che, H.Z.,

732   Zhang, X.Y.: Analysis of the spatiotemporal changes in global land cover from 2001 to 2020,

733   Sci. Total Environ., 908, 168354, https://doi.org/10.1016/j.scitotenv.2023.168354, 2024.

734   Knapp, A., Fay, P.A., Blair, J.M., Collins, S., Smith, M.D., Carlisle, J.D., Harpper, C.W., Danner,

735   B.T., Lett, M.S., Mccarron, J.: Rainfall variability, carbon cycling, and plant species diversity in

736   a mesic grassland, Science, 298, 2202−2205, https://doi.org/10.1126/science.1076347, 2002.

737   Kato, T., Tang, Y.H., Gu, S., Hirota, M., Du, M.Y., Li, Y.N., Zhao, X.Q.: Temperature and biomass

738   influences on interannual changes in CO_2 exchange in an alpine meadow on the Qinghai-Tibetan

739   Plateau, Global Change Biol, 12, 1285−1298, https://doi.org/10.1111/j.1365-

740   2486.2006.01153.x, 2006.

741   Kannenberg, S.A., Anderegg, W.R.L., Barnes, M.L., Dannenberg, M.P., Knapp, A.K.: Dominant

742   role of soil moisture in mediating carbon and water fluxes in dryland ecosystems, Nat. Geosci,

743   17, 38–43, https://doi.org/10.1038/s41561-023-01351-8, 2024.

744   Law, B.E., Falge, E., Gu, L., Baldocchi, D.D., Bakwin, P., Berbigier, P., Davis, K., Dolman, A.J.,

745   Falk, M., Fuentes, J.D., Goldstein, A., Granier, A., Grelle, A., Hollinger, D., Janssens, I.A.,

746   Jarvis, P., Jensen, N.O., Katul, G., Mahli, K., Matteucci, G., Meyers, T., Monson, R., Munger,

747   W., Oechel, W., Olson, R., Pilegaard, K., Paw U, K. T., Thorgeirsson, H., Valentini, R., Verma,
748   Shashi., Vesala, T., Wilson, K., Wofsy, S.: Environmental controls over carbon dioxide and water
749   vapor exchange of terrestrial vegetation, Agric. For. Meteorol, 113, 97–120,
750   https://doi.org/10.1016/S0168-1923(02)00104-1, 2002.

751 Li, S.G., Asanuma, J., Eugster, W., Kotani, A., Liu, J.J., Urano, T., Oikawa, T., Davaa, G.,
752   Oyunbaatar, D., Sugita, M.: Net ecosystem carbon dioxide exchange over grazed steppe in
753   central Mongolia, Global Change Biol, 11, 1941–1955, https://doi.org/10.1111/j.1365-
754   2486.2005.01047.x, 2005.

755 Livesley, S. J., Grover, S., Hutley, L.B., Jamali, H., Butterbach-Bahl, K., Fest, B., Arndt, S. K.:
756   Seasonal variation and fire effects on CH_4, N_2O and CO_2 exchange in savanna soils of northern
757   Australia, Agric. For. Meteorol, 151, 1440–1452,
758   https://doi.org/10.1016/j.agrformet.2011.02.001, 2011.

759 Li, J.X., Zeng, H., Zhu, J.T., Zhang, Y.J., Chen, N., Liu, Y.J.: Responses of different experimental
760   warming on ecosystem respiration in Tibetan alpine meadow, Ecol. Environ. Sci, 25, 1612–1620,
761   https://doi.org/10.16258/j.cnki.1674-5906.2016.10.004, 2016.

762 Li, G.Y., Han, H.Y., Du, Y., Hui, D.F., Xia, J.Y., Niu, S.L., Li, X.N., Wan, S.Q.: Effects of warming
763   and increased precipitation on net ecosystem productivity: a long-term manipulative experiment
764   in a semiarid grassland, Agric. For. Meteorol, 232, 359−366,
765   http://dx.doi.org/10.1016/j.agrformet.2016.09.004, 2017.

766 Liu, D., Li, Y., Wang, T., Peylin, P., MacBean, N., Ciais, P., Jia, G., Ma, M.G., Ma, Y.M., Shen,
767   M.G., Zhang, X.Z., Piao, S.L.: Contrasting responses of grassland water and carbon exchanges
768   to climate change between Tibetan Plateau and InnerMongolia, Agric. For. Meteorol, 249, 163–
769   175, https://doi.org/10.1016/j.agrformet. 2017.11.034, 2018.

770 Lee, E., Kumar, P., Barron-Gafford, G.A., Hendryx, S.M., Sanchez-Cañete, E.P., Minor, R.L.,
771   Colella, T., Scott, R.L.: Impact of hydraulic redistribution on multispecies vegetation water use
772   in a semiarid savanna ecosystem: an experimental and modeling synthesis, Water Resour. Res,
773   54, 4009–4027, https://doi.org/10.1029/2017WR021006, 2018.

774 Liu, J.X., Wang, Z., Duan, Y.F., Li, X.R., Zhang, M.Y., Liu, H.Y., Xue, P., Gong, H.B., Wang, X.,
775   Chen, Y., Geng, Y.N.: Effects of land use patterns on the interannual variations of carbon sinks
776   of terrestrial ecosystems in China, Ecol. Indic, 146, 109914,
777   https://doi.org/10.1016/j.ecolind.2023.109914, 2023.

778 Liu, Z.G., Chen, Z., Yang, M., Hao, T.X., Yu, G.R., Zhu, X.J., Zhang, W.K., Ma, L.X., Dou, X.J.,
779   Lin, Y., Luo, W.X., Han, L., Sun, M.Y., Chen, S.P., Dong, G., Gao, Y.H., Hao, Y.B., Jiang, S.C.,
780   Li, Y.N., Li, Y.Z., Liu, S.M., Shi, P.L., Tang, Y.K., Xin, X.P., Zhang, F.W., Zhang, Y.J., Zhao, L.,
781   Zhou, L., Zhu, Z.L.: Precipitation consistently promotes, but temperature oppositely drives
782   carbon fluxes in temperate and alpine grasslands in China, Agric. For. Meteorol, 344, 109811,
783   https://doi.org/10.1016/j.agrformet.2023.109811, 2024.

784 Miranda, A.C., Miranda, H.S., Lloyd, J., Grace, J., Francey, R.J., McIntyre, J.A., Meir, P., Riggan,
785   P., Lockwood, R., Brass, J.: Fluxes of carbon, water and energy over Brazilian cerrado, an
786   analysis using eddy covariance and stable isotopes, Plant Cell Environ, 20, 315–328,
787   https://doi.org/10.1046/j.1365-3040.1997.d01-80.x, 1997.

788 Malhi, Y., Nobre, A., Grace, J., Kruijt, B., Pereira, M., Culf, A., Scott, S.: Carbon dioxide transfer
789   over a central Amazonian rain forest, J. Geophys. Res, 103, 31593–31612,
790   https://doi.org/10.1029/98JD02647, 1998.

791 Ma, S.Y., Baldocchi, D.D., Xu, L.K., Hehn, T.: Inter-annual variability in carbon dioxide exchange
792   of an oak/grass savanna and open grassland in California, Agric. For. Meteorol, 147, 157–171.
793   https://doi.org/10.1016/j.agrformet.2007.07.008, 2007.

794 Millard, P., Midwood, A. J., Hunt, J.E., Whitehead, D., Boutton, T.W.: Partitioning soil surface CO_2
795   efflux into autotrophic and heterotrophic components, using natural gradients in soil $\delta^{13}C$ in an
796   undisturbed savannah soil, Soil Biol. Biochem, 40, 1575–1582,
797   https://doi.org/10.1016/j.soilbio.2008.01.011, 2008.

798 McDowell, N.G., Allen, C.D.: Darcy's law predicts widespread forest mortality under climate
799   warming, Nat. Clim. Change, 5, 669–72, https://doi.org/10.1038/nclimate2641, 2015.

800 Mattos, C.R.C., Hirota, M., Oliveira, R.S., Flores, B.M., Miguez-Macho, G., Pokhrel, Y., Fan, Y.:
801   Double stress of waterlogging and drought drives forest–savanna coexistence, PNAS, 120,
802   e2301255120, https://doi.org/10.1073/pnas.2301255120, 2023.

803 Niu, S.L., Wu, M.Y., Han, Y., Xia, J.Y., Li, L.H., Wan, S.Q.: Water-mediated responses of ecosystem
804   carbon fluxes to climatic change in a temperate steppe, New Phytol, 177, 209−219,
805   https://doi.org/10.1111/j.1469-8137. 2007.02237.x, 2017.

806 Novick, K.A., Miniat, C.F., Vose, J.M.: Drought limitations to leaf-level gas exchange: results from
807   a model linking stomatal optimization and cohesion–tension theory, Plant Cell Environ, 39, 583–
808   96, https://doi.org/10.1111/pce.12657, 2016.

809 Niu, Y.Y., Li, Y.Q., Wang, X.Y., Gong, X.W., Luo, Y.Q., Tian, D.Y.: Characteristics of annual
810   variation in net carbon dioxide flux in a sandy grassland ecosystem during dry years, Acta
811   Prataculturae Sin, 27, 215–221, https://doi.org/10.11686/cyxb2017231, 2018.

812 Peel, M.C., Finlayson, B.L., McMahon, T.A.: Updated world map of the Köppen-Geiger climate
813   classification, Hydrol. Earth Syst, Sci. 11, 1633–1644, https://doi.org/10.5194/hess-11-1633-
814   2007, 2007.

815 Piao, S.L., Huang, M.T., Liu, Z., Wang, X.H., Ciais, P., Canadell, J.G., Wang, K., Bastos, A.,
816   Friedlingstei, P., Houghto, R.A., Quéré, C.L., Liu, Y.W., Myneni, R.B., Peng, S.S., Pongratz, J.,
817   Sitch, S., Yan, T., Wang, Y.L., Zhu, Z.C., Wu, D.H., Wang, T.: Lower land-use emissions
818   responsible for increased net land carbon sink during the slow warming period, Nat. Geosci. 11,
819   739–743, https://doi.org/10.1038/s41561-018-0204-7, 2018.

820 Pan, S.F., Yang, J., Tian, H.Q., Shi, H., Chang, J.F., Ciais, P., Francois, L., Frieler, K., Fu, B.J.,
821   Hickler, T., Ito, A., Nishina, K., Ostberg, S., Reyer, C.P.O., Schaphoff, S., Steinkamp, J., Zhao,
822   F.: Climate extreme versus carbon extreme: responses of terrestrial carbon fluxes to temperature
823   and precipitation, J. Geophys. Res.: Biogeosci, 125, e2019JG005252,
824   https://doi.org/10.1029/2019JG005252, 2020.

825 Quansah, E., Mauder, M., Balogun, A.A., Amekudz, L.K., Hingerl, L., Bliefernicht, J., Kunstmann,
826   H.: Carbon dioxide fluxes from contrasting ecosystems in the Sudanian savanna in West Africa,
827   Carbon Balance Manage, 10, 1, https://doi.org/10.1186/s13021-014-0011-4, 2015.

828 Ruimy, A., Jarvis, P.G., Baldocchi, D.D., Saugier, B.: CO_2 fluxes over plant canopies and solar
829   radiation: a review, Adv. Ecol. Res, 26, 1–68, https://doi.org/10.1016/s0065-2504(08)60063-x,
830   1995.

831 Santos, A.J.B., Silva, G.T.D.A., Miranda, H.S., Miranda, A.C., Lloyd, J.: Effects of fire on surface
832   carbon, energy and water vapour fluxes over campo sujo savanna in central Brazil, Funct. Ecol,
833   17, 711−719, https://doi.org/10.1111/j.1365-2435.2003.00790.x, 2003.

834 Saleska, S.R., Millar, S.D., Martos, D.M., Goulden, M.L., Wofsy, S.C., da Rocha, H.R., De Camargo,

835   P.B., Crill, P., Daule, B.C., De Freitas, H.C., Hutyra, L., Keller, M., Kirchhoff, V., Menton, M.,
836   Munger, J.W., Pyle, E.H., Rice, A.H., Silva, H.: Carbon in Amazon forests: unexpected seasonal
837   fluxes and disturbance-induced losses, Science, 302, 1554–1557,
838   https://doi.org/10.1126/science.1091165, 2003.

839   Serrano-Ortiz, P., Domingo, F., Cazorla, A., Were, A., Cuezva, S., Villagarcía, L., Alados-Arboledas,
840   L., Kowalski, A.S.: Interannual CO_2 exchange of a sparse mediterranean shrubland on a
841   carbonaceous substrate, J. Geophys. Res.: Biogeosci, 114, https://doi.org/Artn
842   G0401510.1029/2009jg000983, 2009.

843   Shen, R., Zhang, J.L., He, B., Li, F., Zhang, Z.M., Zhou, R., Ou, X.K.: The structure characteristic
844   and analysis on similarity of grassland community in dry-hot valley of Yuanjiang, Ecol.   Environ.
845   Sci, 19, 2821−2825, https://doi.org/10.16258/j.cnki.1674-5906.2010.12.011, 2010.

846   Sulman, B.N., Roman, D.T., Yi, K., Wang, L.X., Phillips, R.P., Novick, K.A.: High atmospheric
847   demand for water can limit forest carbon uptake and transpiration as severely as dry soil,
848   Geophys. Res. Lett, 43, 9686–95, https://doi.org/10.1002/2016GL069416, 2016.

849   Sun, S.S., Wu, Z.P., Xiao, Q.T., Yu, F., Gu, S.H., Fang, D., Li, L., Zhao, X.B.: Factors influencing
850   CO_2, fluxes of a grassland ecosystem on the Yunnan-Guizhou Plateau, China, Acta Prataculturae
851   Sin, 29, 184–191, https://doi.org/10.7522/.10.11686/cyxb2019410, 2020.

852   Sha, Z.Y., Bai, Y.F., Li, R.R., Lan, H., Zhang, X.L., Li, J., Liu, X.F., Chang, S.J., Xie, Y.C.: The
853   global carbon sink potential of terrestrial vegetation can be increased substantially by optimal
854   land management, Commun. Earth Environ, 3, 8, https://doi. 10.1038/s43247-021-00333-1,
855   2022.

856   Tagesson, T., Fensholt, R., Cropley, F., Guiro, I., Horion., S. Ehammer. A., Ardö., J.: Dynamics in
857   carbon exchange fluxes for a grazed semi-arid savanna ecosystem in West Africa, Agric. Ecosyst.
858   Environ, 205, 15–24, https://doi.org/10.1016/j.agee.2015.02.017, 2015.

859   Taylor, P.G., Cleveland, C.C., Wieder, W.R., Sullivan, B.W., Doughty, C.E., Dobrowski, S.Z.,
860   Townsend, A.R.: Temperature and rainfall interact to control carbon cycling in tropical forests,
861   Ecol. Lett. 20, 779–788, https://doi.org/ 10.1111/ele.12765, 2017.

862   Tarin, T., Nolan, R.H., Eamus, D., Cleverly, J.: Carbon and water fluxes in two adjacent Australian
863   semi-arid ecosystems, Agric. For. Meteorol, 281, 107853,
864   https://doi.org/10.1016/j.agrformet.2019.107853, 2020.

865   Veenendaal, E.M., Kolle, O., Lloyd, J.: Seasonal variation in energy fluxes and carbon dioxide
866   exchange for a broad-leaved semiarid savanna (Mopane woodland) in Southern Africa, Global
867   Change Biol, 10, 318–328, https://doi.org/10.1111/j.1365-2486.2003.00699.x, 2004.

868   Woodwell, G.M., Hobbie, J.E., Houghton, R.A., Melillo, J.M., Mooer, B., Peterson, B.J., Shaver,
869   G.R.: Global deforestation: contribution to atmospheric carbon dioxide, Science, 222, 1081–
870   1086, https://doi.org/10.1126/science.222.4628.1081, 1983.

871   White, R.P., Murray, S., Rohweder, M.: Pilot analysis of global ecosystems: grassland ecosystems,
872   World Resources Institute, Washington, DC, http://www. wri.org/wr2000, 2000.

873   Weltzin, J.F., Loik, M.E., Schwinning, S., Williams, D.G., Fay, P.A., Haddad, B.M., Harte, J.,
874   Huxman, T.E., Knapp, A.K., Lin, G.H., Pockman, W.T., Shaw, R.M., Small, E.E., Smith, M.D.,
875   Smith, S.D., Tissue, D.T., Zak, J.C.: Assessing the response of terrestrial ecosystems to potential
876   changes in precipitation, BioScience, 53, 941−952, https://doi.org/10.1641/0006-
877   3568(2003)053[0941:ATROTE]2.0.CO;2, 2003.

878   Wen, X.F., Sun, X.M., Liu, Y.F., Li, X.B.: Effect of linear and exponential fitting on the initial rate

879 of change in CO_2 concentration across the soil surface, Chin. J. Plant Ecol, 31, 380–385,
880 https://doi.org/10.17521/cjpe.2007.0046, 2007.

881 Williams, A.P., Allen, C.D., Macalady, A.K., Griffin, D., Woodhouse, C.A., Meko, D.M., Swetnam,
882 T.W., Rauscher, S.A., Seager, R., Grissino-Mayer, H.D., Dean, J.S., Cook, E.R.,
883 Gangodagamage, C., Cai, M., McDowell, N.G.: Temperature as a potent driver of regional forest
884 drought stress and tree mortality, Nat. Clim. Change, 3, 292–297,
885 https://doi.org/10.1038/nclimate1693, 2013.

886 Wang, W.Y., Guo, J.X., Wang, Y.S., Wu, K.: Observing characteristics of CO_2 flux and its
887 influencing factors over Xilinhot grassland, J. Meteorol. Sci, 35, 100–107, https://doi.org/10.
888 3969 /2013jms. 0065, 2015.

889 Wu, F.T., Cao, S.K., Cao, G.C., Han, G.Z., Lin, Y.Y., Cheng, S.Y.: Variation of CO_2 flux of alpine
890 wetland ecosystem of *Kobresta tibetica* wet meadow in Lake Qinghai, J. Ecol. Rural Environ,
891 34, 124–131, https://doi.org/10.11934/1.19n.1673-4831.2018.02.004, 2018.

892 Wang, N., Quesada, B., Xia, L.L., Butterbach-Bahl, K., Goodale, C.L., Kiese, R.: Effects of climate
893 warming on carbon fluxes in grasslands – a global meta-analysis, Global Change Biol, 25, 1839–
894 1851, https://doi.org/10.1111/gcb.14603, 2019.

895 Wang, Y.Y., Xiao, J.F., Ma, Y.M., Luo, Y.Q., Hu, Z.Y., Li, F., Li Y.N., Gu, L.L., Li, Z.G., Yuan, L.:
896 Carbon fluxes and environmental controls across different alpine grassland types on the Tibetan
897 Plateau, Agric. For. Meteorol, 311, 1–14, https://doi.org/10.1016/j.agrformet.2021.108694,
898 2021.

899 Wang, H.H., Huang, W.D., He, Y.Z., Zhu, Y.Z.: Effects of warming and precipitation reduction on
900 soil respiration in Horqin sandy grassland, northern China, Catena, 233, 107470,
901 https://doi.org/10.1016/j.catena.2023.107470, 2023.

902 Wang, F., Harindintwali, J.D., Wei, K., Shan, Y.L., Mi, Z.F., Costello, M.J., Grunwald, S., Feng,
903 Z.Z., Wang, F.M., Guo, Y.M., Wu, X., Kumar, P., Kästner, M., Feng, X.J., Kang, S.C., Liu, Z., Fu,
904 Y.H., Zhao, W., Ouyang, C.J., Shen, J.L., Wang, H.J., Chang, S.X., Evans, D.L., Wang, R., Zhu,
905 C.W., Xiang, L.L., Rinklebe, J., Du, M.M., Huang, L., Bai, Z.H., Li, S., Lal, R., Elsner, M.,
906 Wigneron, J.P., Florindo, F., Jiang, X., Shaheen, S.M., Zhong, X.Y., Bol, R., Vasques, G.M., Li,
907 X.F., Pfautsch, S., Wang, M.G., He, X., Agathokleous, E., Du, H.B., Kengara, F.O., Brahushi, F.,
908 Long, X.E., Pereira, P., Ok, Y.S., Rillig, M.C., Jeppesen, E., Barceló, D., Yan, X.Y., Jiao, N.Z.,
909 Han, B.X., Schäffer, A., Chen, J.M., Zhu, Y.G., Cheng, H., Amelung, W., Spötl, C., Zhu, J.K.,
910 Tiedje, J.M.: Climate change: Strategies for mitigation and adaptation, The Innovation Geosci, 1,
911 100015, https://doi. 10.59717/j.xinn-geo.2023.100015, 2023.

912 Xiang, Y.B., Zhou, S.X., Xiao, Y.X., Hu, T.X., Tu, L.H., Huang, C.D.: Effects of precipitation
913 variations on soil respiration in an evergreen broad-leaved forest during dry and wet seasons,
914 Acta Ecol. Sin., 37, 4734−4742, https://doi.org/ 10.5846/stxb201604160701, 2017.

915 Xu, X.L: China watershed and river network datasets based on DEM extraction, Resource and
916 Environmental Science Data Registration and Publishing System [data set],
917 https://doi.org/10.12078/2018060101, 2018.

918 Xu, X.L: China's multi-year provincial administrative division boundary data, Resource and
919 Environmental Science Data Registration and Publishing System [data set],
920 https://doi.org/10.12078/2023010103, 2023a.

921 Xu, X.L: China's multi-year county administrative division boundary data, Resource and
922 Environmental Science Data Registration and Publishing System [data set],

923   https://doi.org/10.12078/2023010101, 2023b.

924 Xu, Y.N., Wang, X., Sun, Y.R., Liu, H.T., Li, L., Schäufele, R., Gong, X.Y.: Response of
925   photosynthetic ^{13}C discrimination to vapour pressure deficit reflects changes in bundle-sheath
926   leakiness in two C_4 grasses, Environ. Exp. Bot, 216, 105529,
927   https://doi.org/10.1016/j.envexpbot.2023.105529, 2023.

928 Yang, Z.P., Chang, Y.: Ecological problems of primary dry valleys is southwest China and advances
929   in the researches into them, Agric. Res. Arid Areas, 25, 90−93, 2007.

930 Yu, K., D'Odorico, P.: Hydraulic lift as a determinant of tree–grass coexistence on savannas, New
931   Phytol, 207, 1038–1051, https://doi.org/10.1111/nph.13431, 2015.

932 Yuan, W.P., Zheng, Y., Piao, S.L., Ciais, P., Lombardozzi, D., Wang, Y.P., Ryu, Y., Chen, G.X., Dong,
933   W.J., Hu, Z.M., Jain, A.K., Jiang, C.Y., Kato, E., Li, S.H., Lienert, S., Liu, S.G., Nabel, J.E.M.S.,
934   Qin, Z.C., Quine, T., Sitch, S., Smith, W.K., Wang, F., Wu, C.Y., Xiao, Z.Q., Yang, S.: Increased
935   atmospheric vapor pressure deficit reduces global vegetation growth, Sci. Adv, 5, eaax1396,
936   https://doi.org/10.1126/sciadv.aax1396, 2019.

937 Yang, K.Y., Gong, H.D., Li, J., Liu, Y.T., Sha, L.Q., Song, Q.H., Jin, Y.Q., Yang, D.X., Li, P.G., Wen,
938   G.J., Chen, A.G., Pang, Z.Q., Zhang, Y.P.: Dynamic characteristics of soil respiration of savanna
939   ecosystem in dry hot valley of Yuanjiang, J. Zhejiang Agric. For. Univ, 37, 849–859,
940   https://doi.org/10.11833/j.issn.2095-0756.20190647, 2020.

941 Yang, Y.H., Shi, Y., Sun, W.J., Chang, J.F., Zhu, J.X., Chen, L.Y., Wang, X., Guo, Y.P., Hongtu, Z.,
942   Yu, L.F., Zhao, S.Q., Xu, K., Zhu, J.L., Shen, H.H., Wang, Y.Y., Peng, Y.F., Zhao, X., Wang, X.Q.,
943   Hu, H.F., Chen, S.Q., Huang, M., Wen, X.F., Wang, S.P., Zhu, B., Niu, S.L., Tang, Z.Y., Liu, L.L.,
944   Fang, J.Y.: Terrestrial carbon sinks in China and around the world and their contribution to carbon
945   neutrality, Sci. China Life Sci, 65, 861−895, https://doi.org/10.1007/s11427-021-2045-5, 2022.

946 Zhang, R.Z.: The dry valley of the Henduan Mountains region, Beijing Sci. Press, ISBN
947   703002916X, 1992.

948 Zhao, L., Gu, S., Xu, S.X., Zhao, X.Q., Li, Y.N.: Carbon flux and controlling process of alpine
949   meadow on Qinghai-Tibetan plateau, Acta Botan. Boreali-Occidentalia Sin, 27, 1054–1060,
950   2007.

951 Zhang, F.W., Li, Y.N., Cao, G.M., Li, F.X., Ye, G.J., Liu, J.H., Wei, Y.L., Zhao, X.Q.: CO_2 fluxes
952   and their driving factors over alpine meadow grassland ecosystems in the northern shore of
953   Qinghai Lake, China, Chin. J. Plant Ecol, 36,187–198,
954   https://doi.org/10.3724/SP.J.1258.2012.00187, 2012.

955 Zou, H., Gao, G.Y., Fu, B.J.: The relationship between grassland ecosystem and soil water in arid
956   and semi-arid areas: a review, Acta Ecol. Sin, 36, 3127–3136,
957   https://doi.org/10.5846/stxb201506211251, 2016.

958 Zhang, W.M., Brandt, M., Penuelas, J., Guichard, F., Tong, X., Tian, F., Fensholt, R.: Ecosystem
959   structural changes controlled by altered rainfall climatology in tropical savannas, Nat.
960   Commun, 10, 671, https://doi.org/10.1038/s41467-019-08602-6, 2019.

961 Zhang, R., Zhao, X.Y., Zuo, X.A., Qu, H., Degen, A.A., Luo, Y.Y., Ma, X.J., Chen, M., Liu, L.X.,
962   Chen, J.L.: Impacts of precipitation on ecosystem carbon fluxes in desert−grasslands in Inner
963   Mongolia, China, J. Geophys. Res. Atmos, 124, 1266−1276,
964   https://doi.org/10.1029/2018JD028419, 2019.

965 Zhao, H.C., Jia, G.S., Wang, H.S., Zhang, A.Z., Xu, X.Y.: Diurnal variations of the carbon fluxes of
966   semiarid meadow steppe and typical steppe in China, Clim. Environ. Res, 25, 172–184,

967   https://doi.org/10.3878/j.issn.1006-9585.2019.19096, 2020.

968 Zhang, Y.J., Qiu, L.P., Gao, H.L., Liu. J., Wei, X.R., Zhang, X.C.: Responses of ecosystem CO_2
969   exchange to clipping in a semi-arid typical grassland on the Loess Plateau, Acta Ecol. Sin, 40,
970   336–344, https://doi.org/10.5846/stxb201810172244, 2020.

971 Zeng, Z.Q., Wu, W.X., Li, Y.M., Huang, C., Zhang, X.Q., Peñuelas, J., Zhang, Y., Gentine, P., Li,
972   Z.L., Wang, X.Y., Huang, H., Ren, X.S., Ge, Q.S.: Increasing meteorological drought under
973   climate change reduces terrestrial ecosystem productivity and carbon storage, One Earth, 6,
974   1326–1339, https://doi.org/10.1016/j.oneear.2023.09.007, 2023.

975 Zhou, Y., Bomfim, B., Bond, W.J., Boutton, T.W., Case, M.F., Coetsee, C., Davies, A.B., February,
976   E.C., Gray, E.F., Silva, L.C.R., Wrigh, J., Staver, A.C.: Soil carbon in tropical savannas mostly
977   derived from grasses, Nat. Geosci, 16, 710−716, https://www.nature.com/articles/s41561-023-
978   01232-0, 2023.

979 Zhong, Z.Q., He, B., Wang, Y.P., Chen, H.W., Chen, D.L., Fu, Y.S.H., Chen, Y.N., Guo, L.L., Deng,
980   Y., Huang, L., Yuan, W.P., Hao, X.M., Tang, R., Liu, H.M., Sun, L.Y., Xie, X.M., Zhang, Y.F.:
981   Disentangling the effects of vapor pressure deficit on northern terrestrial vegetation productivity,
982   Sci. Adv, 9, eadf3166, https://doi.org/10.1126/sciadv.adf3166, 2023.